National Library
of Canada

Acquisitions and
Bibliographic Services Branch

395 Wellington Street
Ottawa, Ontario
K1A 0N4

Bibliothèque nationale
du Canada

Direction des acquisitions et
des services bibliographiques

395, rue Wellington
Ottawa (Ontario)
K1A 0N4

Your file Votre référence

Our file Notre référence

NOTICE

The quality of this microform is heavily dependent upon the quality of the original thesis submitted for microfilming. Every effort has been made to ensure the highest quality of reproduction possible.

If pages are missing, contact the university which granted the degree.

Some pages may have indistinct print especially if the original pages were typed with a poor typewriter ribbon or if the university sent us an inferior photocopy.

Reproduction in full or in part of this microform is governed by the Canadian Copyright Act, R.S.C. 1970, c. C-30, and subsequent amendments.

AVIS

La qualité de cette microforme dépend grandement de la qualité de la thèse soumise au microfilmage. Nous avons tout fait pour assurer une qualité supérieure de reproduction.

S'il manque des pages, veuillez communiquer avec l'université qui a conféré le grade.

La qualité d'impression de certaines pages peut laisser à désirer, surtout si les pages originales ont été dactylographiées à l'aide d'un ruban usé ou si l'université nous a fait parvenir une photocopie de qualité inférieure.

La reproduction, même partielle, de cette microforme est soumise à la Loi canadienne sur le droit d'auteur, SRC 1970, c. C-30, et ses amendements subséquents.

Canada

UNIVERSITY OF ALBERTA

Calibration Techniques for Camera and Robot Manipulator

BY

Kavita Ravi

A thesis submitted to the Faculty of Graduate Studies and Research in partial fulfillment of the requirements for the degree of Master of Science.

DEPARTMENT OF COMPUTING SCIENCE

Edmonton, Alberta
Fall 1994

National Library
of Canada

Acquisitions and
Bibliographic Services Branch

395 Wellington Street
Ottawa, Ontario
K1A 0N4

Bibliothèque nationale
du Canada

Direction des acquisitions et
des services bibliographiques

395, rue Wellington
Ottawa (Ontario)
K1A 0N4

Your file Votre référence

Our file Notre référence

The author has granted an irrevocable non-exclusive licence allowing the National Library of Canada to reproduce, loan, distribute or sell copies of his/her thesis by any means and in any form or format, making this thesis available to interested persons.

L'auteur a accordé une licence irrévocable et non exclusive permettant à la Bibliothèque nationale du Canada de reproduire, prêter, distribuer ou vendre des copies de sa thèse de quelque manière et sous quelque forme que ce soit pour mettre des exemplaires de cette thèse à la disposition des personnes intéressées.

The author retains ownership of the copyright in his/her thesis. Neither the thesis nor substantial extracts from it may be printed or otherwise reproduced without his/her permission.

L'auteur conserve la propriété du droit d'auteur qui protège sa thèse. Ni la thèse ni des extraits substantiels de celle-ci ne doivent être imprimés ou autrement reproduits sans son autorisation.

ISBN 0-315-95102-8

Canada

Name KAVITA RAVI

Dissertation Abstracts International is arranged by broad, general subject categories. Please select the one subject which most nearly describes the content of your dissertation. Enter the corresponding four-digit code in the spaces provided.

SUBJECT TERM

SUBJECT CODE 0984 U·M·I

Subject Categories

THE HUMANITIES AND SOCIAL SCIENCES

COMMUNICATIONS AND THE ARTS
Architecture 0729
Art History 0377
Cinema 0900
Dance 0378
Fine Arts 0357
Information Science 0723
Journalism 0391
Library Science 0399
Mass Communications 0708
Music 0413
Speech Communication 0459
Theater 0465

EDUCATION
General 0515
Administration 0514
Adult and Continuing 0516
Agricultural 0517
Art 0273
Bilingual and Multicultural 0282
Business 0688
Community College 0275
Curriculum and Instruction 0727
Early Childhood 0518
Elementary 0524
Finance 0277
Guidance and Counseling 0519
Health 0680
Higher 0745
History of 0520
Home Economics 0278
Industrial 0521
Language and Literature 0279
Mathematics 0280
Music 0522
Philosophy of 0998
Physical 0523
Psychology 0525
Reading 0535
Religious 0527
Sciences 0714
Secondary 0533
Social Sciences 0534
Sociology of 0340
Special 0529
Teacher Training 0530
Technology 0710
Tests and Measurements 0288
Vocational 0747

LANGUAGE, LITERATURE AND LINGUISTICS
Language
- General 0679
- Ancient 0289
- Linguistics 0290
- Modern 0291

Literature
- General 0401
- Classical 0294
- Comparative 0295
- Medieval 0297
- Modern 0298
- African 0316
- American 0591
- Asian 0305
- Canadian (English) 0352
- Canadian (French) 0355
- English 0593
- Germanic 0311
- Latin American 0312
- Middle Eastern 0315
- Romance 0313
- Slavic and East European 0314

PHILOSOPHY, RELIGION AND THEOLOGY
Philosophy 0422
Religion
- General 0318
- Biblical Studies 0321
- Clergy 0319
- History of 0320
- Philosophy of 0322

Theology 0469

SOCIAL SCIENCES
American Studies 0323
Anthropology
- Archaeology 0324
- Cultural 0326
- Physical 0327

Business Administration
- General 0310
- Accounting 0272
- Banking 0770
- Management 0454
- Marketing 0338

Canadian Studies 0385
Economics
- General 0501
- Agricultural 0503
- Commerce-Business 0505
- Finance 0508
- History 0509
- Labor 0510
- Theory 0511

Folklore 0358
Geography 0366
Gerontology 0351
History
- General 0578
- Ancient 0579
- Medieval 0581
- Modern 0582
- Black 0328
- African 0331
- Asia, Australia and Oceania 0332
- Canadian 0334
- European 0335
- Latin American 0336
- Middle Eastern 0333
- United States 0337

History of Science 0585
Law 0398
Political Science
- General 0615
- International Law and Relations 0616
- Public Administration 0617

Recreation 0814
Social Work 0452
Sociology
- General 0626
- Criminology and Penology 0627
- Demography 0938
- Ethnic and Racial Studies 0631
- Individual and Family Studies 0628
- Industrial and Labor Relations 0629
- Public and Social Welfare 0630
- Social Structure and Development 0700
- Theory and Methods 0344

Transportation 0709
Urban and Regional Planning 0999
Women's Studies 0453

THE SCIENCES AND ENGINEERING

BIOLOGICAL SCIENCES
Agriculture
- General 0473
- Agronomy 0285
- Animal Culture and Nutrition 0475
- Animal Pathology 0476
- Food Science and Technology 0359
- Forestry and Wildlife 0478
- Plant Culture 0479
- Plant Pathology 0480
- Plant Physiology 0817
- Range Management 0777
- Wood Technology 0746

Biology
- General 0306
- Anatomy 0287
- Biostatistics 0308
- Botany 0309
- Cell 0379
- Ecology 0329
- Entomology 0353
- Genetics 0369
- Limnology 0793
- Microbiology 0410
- Molecular 0307
- Neuroscience 0317
- Oceanography 0416
- Physiology 0433
- Radiation 0821
- Veterinary Science 0778
- Zoology 0472

Biophysics
- General 0786
- Medical 0760

EARTH SCIENCES
Biogeochemistry 0425
Geochemistry 0996
Geodesy 0370
Geology 0372
Geophysics 0373
Hydrology 0388
Mineralogy 0411
Paleobotany 0345
Paleoecology 0426
Paleontology 0418
Paleozoology 0985
Palynology 0427
Physical Geography 0368
Physical Oceanography 0415

HEALTH AND ENVIRONMENTAL SCIENCES
Environmental Sciences 0768
Health Sciences
- General 0566
- Audiology 0300
- Chemotherapy 0992
- Dentistry 0567
- Education 0350
- Hospital Management 0769
- Human Development 0758
- Immunology 0982
- Medicine and Surgery 0564
- Mental Health 0347
- Nursing 0569
- Nutrition 0570
- Obstetrics and Gynecology 0380
- Occupational Health and Therapy 0354
- Ophthalmology 0381
- Pathology 0571
- Pharmacology 0419
- Pharmacy 0572
- Physical Therapy 0382
- Public Health 0573
- Radiology 0574
- Recreation 0575
- Speech Pathology 0460
- Toxicology 0383

Home Economics 0386

PHYSICAL SCIENCES
Pure Sciences
Chemistry
- General 0485
- Agricultural 0749
- Analytical 0486
- Biochemistry 0487
- Inorganic 0488
- Nuclear 0738
- Organic 0490
- Pharmaceutical 0491
- Physical 0494
- Polymer 0495
- Radiation 0754

Mathematics 0405
Physics
- General 0605
- Acoustics 0986
- Astronomy and Astrophysics 0606
- Atmospheric Science 0608
- Atomic 0748
- Electronics and Electricity 0607
- Elementary Particles and High Energy 0798
- Fluid and Plasma 0759
- Molecular 0609
- Nuclear 0610
- Optics 0752
- Radiation 0756
- Solid State 0611

Statistics 0463

Applied Sciences
Applied Mechanics 0346
Computer Science 0984
Engineering
- General 0537
- Aerospace 0538
- Agricultural 0539
- Automotive 0540
- Biomedical 0541
- Chemical 0542
- Civil 0543
- Electronics and Electrical 0544
- Heat and Thermodynamics 0348
- Hydraulic 0545
- Industrial 0546
- Marine 0547
- Materials Science 0794
- Mechanical 0548
- Metallurgy 0743
- Mining 0551
- Nuclear 0552
- Packaging 0549
- Petroleum 0765
- Sanitary and Municipal 0554
- System Science 0790

Geotechnology 0428
Operations Research 0796
Plastics Technology 0795
Textile Technology 0994

PSYCHOLOGY
General 0621
Behavioral 0384
Clinical 0622
Developmental 0620
Experimental 0623
Industrial 0624
Personality 0625
Physiological 0989
Psychobiology 0349
Psychometrics 0632
Social 0451

UNIVERSITY OF ALBERTA

RELEASE FORM

NAME OF AUTHOR: Kavita Ravi

TITLE OF THESIS: Calibration Techniques for Camera and Robot Manipulator

DEGREE: Master of Science

YEAR THIS DEGREE GRANTED: 1994

Permission is hereby granted to the University of Alberta Library to reproduce single copies of this thesis and to lend or sell such copies for private, scholarly or scientific research purposes only.

The author reserves all other publication and other rights in association with the copyright in the thesis, and except as hereinbefore provided neither the thesis nor any substantial portion thereof may be printed or otherwise reproduced in any material form whatever without the author's prior written permission.

(Signed) . . Kavita . . . . . .

Kavita Ravi
Plot 32, G. K. Colony
Secunderabad, A.P.
India – 500 594

Date: . Sept. 29, 1994

UNIVERSITY OF ALBERTA

FACULTY OF GRADUATE STUDIES AND RESEARCH

The undersigned certify that they have read, and recommend to the Faculty of Graduate Studies and Research for acceptance, a thesis entitled **Calibration Techniques for Camera and Robot Manipulator** submitted by Kavita Ravi in partial fulfillment of the requirements for the degree of Master of Science.

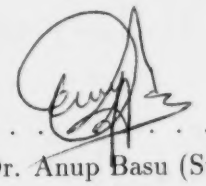

Dr. Anup Basu (Supervisor)

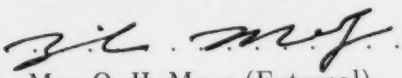

Dr. Max Q.-H. Meng (External)

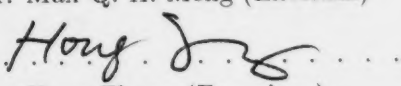

Dr. Hong Zhang (Examiner)

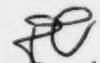

Dr. Pawel Gburzynski (Chair)

Date: SEPT. 23, 1994

To my family

Abstract

This thesis presents new calibration techniques for camera and robot manipulators. Any equipment must be calibrated to achieve accurate functioning. *Camera calibration* is an important process in three-dimensional (3D) vision applications where it is required to relate two-dimensional (2D) images to the 3D world. Camera calibration involves modeling the relationship between the positions of features in 3D space to their corresponding positions in the 2D image. A camera calibration procedure determines the internal geometric and optical parameters, such as, *focal length* and *image center* (intrinsic parameters), and the 3D position and orientation of the camera relative to a world coordinate frame (extrinsic parameters). *Robot calibration* is essential to improve the positioning accuracy of robot manipulators. A mathematical (kinematic) model is used to describe the geometric structure of a robot manipulator. Robot calibration procedure involves calculating and improving the values of this model's parameters.

The camera calibration technique presented in this thesis calibrates the intrinsic parameters. The technique uses an active camera (capable of pan, tilt and roll movements) to capture images. Relationships among these images are represented by linear equations involving the camera parameters, which are then solved. This procedure does not require a pre-defined calibration pattern.

The robot calibration technique presented in this thesis uses a vision system to calibrate the kinematic model. For an n-linked robot manipulator, the procedure cal-

ibrates one link at a time, starting with the n^{th} link by making small movements. The resulting equations are linear, consequently, the algorithms are simple. Experiments were performed, validating the proposed camera and robot calibration techniques.

Acknowledgements

I would like to thank Prof. Anup Basu, my supervisor, for initially suggesting the problem and providing constant guidance, encouragement and support during the course of this research. Anup made sure I progressed at a steady pace in my research and did not stay stuck for too long.

Prof. Hong Zhang read earlier versions of my thesis and provided insightful comments. I thank him for his constructive criticism. Thanks are due to Prof. M. Meng for his careful reading of the thesis. I thank Steve Sutphen for his help in the Robotics and Computer Vision Laboratory, setting up equipment for experiments and providing many helpful suggestions in performing them.

I thank my friends for making the long winters in Edmonton bearable. The support of my family was crucial to the completion of the research and the thesis. Finally, I would like to thank my husband for his support and help during the course of my study.

Contents

1 Introduction **1**

1.1 Camera Calibration 1

1.1.1 Camera Models 2

1.2 Robot Calibration 5

1.2.1 Robot Kinematic Models 7

1.3 Thesis Outline 12

2 Previous Work **14**

2.1 Camera Calibration 14

2.1.1 Pin-hole Model 14

2.1.2 Non-linear Techniques 15

2.1.3 Linear and Partially Linear Techniques 16

2.1.4 Two-plane Model 18

2.2 Robot Calibration 19

2.2.1 General Solution 19

2.2.2 Calibration Techniques 21

2.3 Conclusions 23

3 Active Camera Calibration **24**

3.1 Introduction 24

3.2 Mathematical Derivations 26

3.3 Strategies for Active Calibration 29

3.3.1 Alternative Strategy 32

3.3.2 Alternate Strategy for Computation of Image Center 34

3.4 Theoretical Error Analysis 36

3.5 Conclusions 39

4 Robot Calibration **40**

4.1 Introduction 40

4.2 Camera Extrinsic Calibration 43

4.2.1 Mathematical Derivations 43

4.2.2 Camera Extrinsic Calibration Algorithm 46

4.3 Robot Calibration 47

4.3.1 Mathematical Derivations 48

4.3.2 Robot Calibration Algorithm 53

4.4 Theoretical Error Analysis 53

4.5 Conclusions 54

5 Experimental results **55**

5.1 Active camera calibration 55

5.1.1 Simulations 55

5.1.2 Experiments with Real Images 61

5.2 Robot kinematic calibration 66

5.2.1 Simulations 71

5.3 Conclusions 79

6 Conclusions and Future Directions **80**

6.1 Camera Calibration 80

6.1.1 Advantages and Limitations 81

6.1.2 Future Directions 81

6.2 Robot Calibration 82

6.2.1 Issues 82

6.2.2 Future Directions 83

Bibliography **85**

List of Figures

1.1 The *Pin-hole* Camera Model. 3

1.2 The *Two-plane* Camera Model. 3

1.3 Robot Kinematic Model with Non-geometric Parameters. 8

1.4 The *D-H* Kinematic Model: Four Parameters. 10

1.5 The *Hayati* Kinematic Model: Five Parameters. 11

1.6 The *S-Model*: Six Parameters. 13

3.7 Camera Model: Perspective Projection. 27

3.8 Schematics of an Active Camera. 30

4.9 Eye-in-Hand System. 42

4.10 A Two-link Manipulator with D-H Model Parameters. 48

4.11 Transform Graphs for Movement of Joint 2. 49

4.12 Transform Graphs for Movement of Joint 1. 51

5.13 Variation of Error in Focal Length. 57

5.14 Variation of Error in Focal Length with Noise (Strategy B). 58

5.15 Variation of Error in Image Center with Roll Angle and Noise. 59

5.16 Comparison of Strategy C and Strategy D in Computing Image Center. 60

5.17 Comparison of Strategy C and Strategy D in Computing Focal Length. 60

5.18 Error in δx and δy when Axis of Rotation is Parallel to the Camera z axis. 61

5.19 Error in δx with Error in Axis of Rotation (at an angle to the camera z axis). 62

5.20 Error in δy with Error in Axis of Rotation (at an angle to the camera z axis). 62

5.21 Image Sequence. 63

5.22 Edges of Image Sequence. 64

5.23 Image Sequence. 64

5.24 Edges of Image Sequence. 65

5.25 Sequence of Images Taken (first scene). 67

5.26 Corresponding Edges of the Images (first scene). 68

5.27 Sequence of Images Taken (second scene). 69

5.28 Corresponding Edges of the Images (second scene). 70

5.29 Three Link Robot. 71

5.30 Variation of Error in l_3 with Rotational Errors. 73

5.31 Variation of Error in l_2 with Rotational Errors. 73

5.32 Variation of Error in l_1 with Rotational Errors. 74

5.33 Variation of Error in l_3 with Translational Errors. 74

5.34 Variation of Error in l_2 with Translational Errors. 75

5.35 Variation of Error in l_1 with Translational Errors. 75

5.36 Variation of Error in d_3 with Rotational Errors. 76

5.37 Variation of Error in d_2 with Rotational Errors. 76

5.38 Variation of Error in d_3 with Translational Errors. 77

5.39 Variation of Error in d_2 with Translational Errors. 77

5.40 Variation of Error in α_3 with Rotational Errors. 78

5.41 Variation of Error in α_2 with Rotational Errors. 78

5.42 Variation of Error in α_1 with Rotational Errors. 79

List of Tables

5.1 Simulation Results of Strategy A and B Without Noise. 56

5.2 Simulation Results of Strategy C in Computing Image Center 58

5.3 Simulation Results of Strategy D in Computing Image Center 59

5.4 Simulation Results in Estimating Focal Length 60

5.5 Actual Values of Link Parameters. 71

5.6 Errors in Values of Link Parameters. 72

Chapter 1

Introduction

This thesis deals with two important problems in the area of 3D vision and robotics, namely, camera and robot calibration. Calibration techniques to determine the internal parameters of mathematical models of camera and robot manipulator are discussed. This chapter presents a brief introduction to the calibration problem and describes a few mathematical models to represent a camera and robot manipulator.

1.1 Camera Calibration

Camera calibration is an important process in vision applications where there is a necessity to accurately relate 2D images to the 3D world. These include pose estimation [Linnainmaa et al. 1988], 3D motion estimation, navigation [Turk et al. 1987], automated assembly and other applications of robotic vision. *Camera calibration* involves modeling the relationship between the positions of points in 3D space and their corresponding 2D image. The calibration process, which determines the internal geometric and optical characteristics (intrinsic parameters such as focal length, image center), is *camera intrinsic calibration*. These internal parameters have to be calibrated because manufacturing imperfections cause actual values to differ from ideal

values. The process of identifying the 3D position and orientation (extrinsic parameters) of the camera frame, relative to a world coordinate frame, is *camera extrinsic calibration*. This is usually necessary when the camera is coordinated with other equipment, such as a robot system. The accuracy of the camera model depends on the accuracy of these parameters.

An ideal calibration process would be the one which is autonomous (should not require any manual intervention), reasonably accurate and efficient. Once a camera has been calibrated, the model can be used in two ways [Chang and Liang 1989]:

- *Forward projection*: given the 3D location of a point in space, predict its position in the 2D image.
- *Backward Projection*: given a 2D image point, compute the line of sight ray in 3-D space.

1.1.1 Camera Models

A camera model should be complete, i.e., it should permit both forward and backward projections. Primarily two camera models are used: the *pin-hole* model shown in figure 1.1 and the *two-plane* model, shown in figure 1.2. In the *pin-hole* model, all light rays (lines of sight) from the front of the camera pass through the lens center and are projected onto the image plane at the back of the camera. To avoid dealing with an inverted image, the image plane is considered to be at the front of the camera, at the same distance from the lens as at the back. The distance from the lens center to the image plane is known as the *focal length* (f). The *two-plane* model differs from the pin-hole model in that the lines of sight need not pass through the same point, i.e., there is not necessarily a unique lens center. Images of two calibration planes ($P1$ and $P2$) with known points are extracted. The calibration points are used to interpolate the location of an image point on each plane separately. Let the image point be v and the corresponding locations on the two planes be u_1 and u_2. The

line of sight vector for v is then obtained by connecting u_1 and u_2. Various types of interpolation techniques can be used depending on the accuracy required [Gremban et al. 1988]. With the two-plane model, it is easy to obtain the backward projection but not the forward projection.

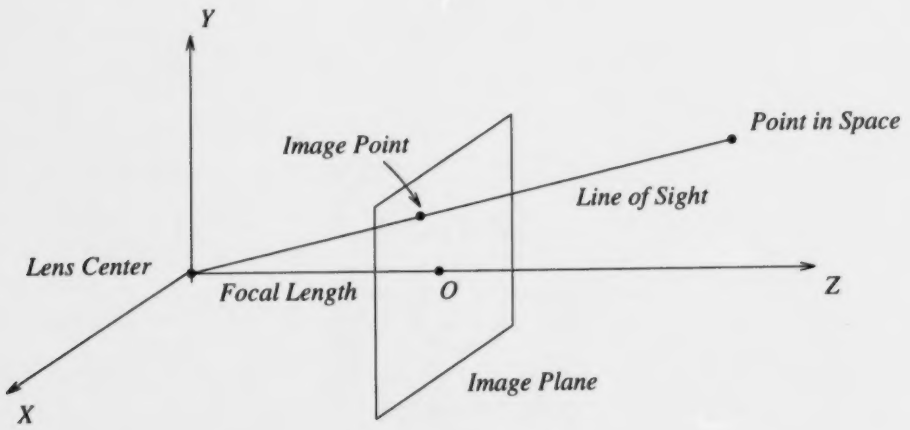

Figure 1.1: The *Pin-hole* Camera Model.

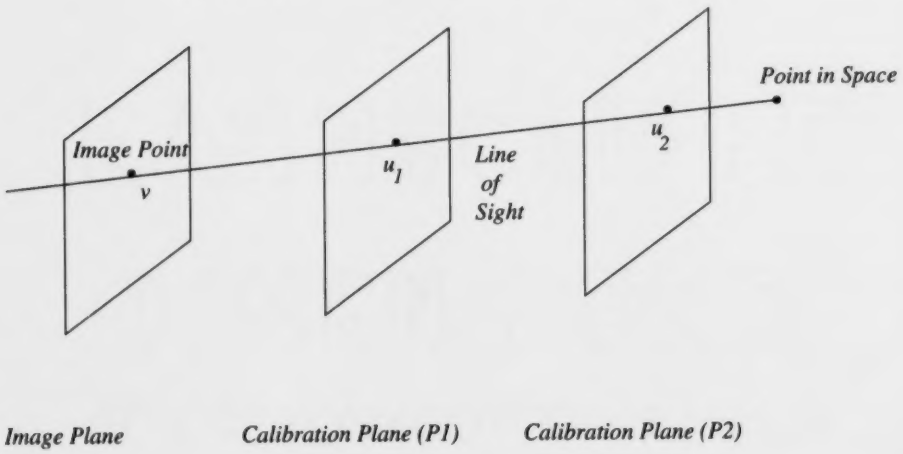

Figure 1.2: The *Two-plane* Camera Model.

The basic pin-hole model is the most commonly used in vision applications. The camera coordinate system is defined as the 3D frame with the lens center as the center, x and y axes parallel to the image plane and z axis along the optical axis (figure 1.1). The main steps of transformation from 3D world coordinate to camera coordinates can be stated as follows [Tsai 1987]:

step 1: *Transform the world coordinate system (X_w, Y_w, Z_w) to camera 3D coordinate system (X_c, Y_c, Z_c)* as,

$$\begin{bmatrix} X_c \\ Y_c \\ Z_c \end{bmatrix} = R \begin{bmatrix} X_w \\ Y_w \\ Z_w \end{bmatrix} + T$$

where R is a 3×3 rotation matrix and T is a translation vector.

The parameters of R and T need to be calibrated if it is necessary to know the location of the camera relative to the world.

step 2: *Transformation from 3D camera coordinate system (X_c, Y_c, Z_c) to the image coordinates (x_u, y_u).* This is given by the pin-hole perspective projection,

$$x_u = f\frac{X_c}{Z_c} \tag{1.1}$$

$$y_u = f\frac{Y_c}{Z_c} \tag{1.2}$$

The internal parameter to be calibrated is the focal length (f).

step 3: *Modeling lens distortion.* There are mainly two kinds of distortions — *radial* and *tangential*. Most applications consider only radial distortion. Radial distortion can be modeled as follows,

$$x_d = x_u(1 + kr^2)^{-1}$$

$$y_d = y_u(1 + kr^2)^{-1}$$

where $r^2 = \sqrt{x_u^2 + y_u^2}$. The parameter to be calibrated is the distortion coefficient (k).

step 4: *Convert from real image coordinates (x_d, y_d) to pixel (digital) coordinates* as,

$$x = s_x x_d + \delta_x$$

$$y = s_y y_d + \delta_y$$

where s_x and s_y are the (usually different) scaling factors along the horizontal and vertical directions. δ_x and δ_y are the distance between the origin of the

image and the intersection of the optical axis with the image plane (the image center) along the x and y directions.

The parameters in steps 1 and 3 need to be determined if external calibration is necessary and lens distortion is present. If only internal calibration is required and lens distortion is negligible, the parameters in steps 2 and 4 need to be determined. In this case, the transformation between the 3D camera coordinates and pixel coordinates can be given as follows,

$$x = f_x \frac{X_c}{Z_c} + \delta_x \tag{1.3}$$

$$y = f_y \frac{Y_c}{Z_c} + \delta_y \tag{1.4}$$

Two focal lengths are used ($f_x = s_x f$, $f_y = s_y f$) throughout this thesis instead of a single focal length (f) and an aspect ratio (the ratio of the y-direction scaling to x-direction scaling).

1.2 Robot Calibration

The performance of a robot system depends on various factors such as the positioning accuracy of the robots and accuracy of sensing devices. *Repeatability* and *Accuracy* are two important measures of robot system performance. A robot's repeatability is the measure of how well the robot can cyclically position itself at a previously taught pose, whereas accuracy is a measure of how precisely the robot can move to a desired pose in the workspace. Since most applications, such as grasping and navigation, require the robot to move along paths which are not previously taught, it is important to consider its accuracy.

A mathematical model, known as the *kinematic model*, is used to represent the robot manipulator, compute the robot joint angles and control the position of the end-effector. The model gives the relationships between successive joint positions.

This information gives the position and orientation of the end-effector relative to the base of the robot as a function of the model parameters. Thus, if Q_1, Q_2, ..., Q_n are parameters of the model, the pose x (position and orientation) of the robot is the function,

$$x = f(Q_1, Q_2, ..., Q_n)$$

Thus the position accuracy of a robotic manipulator depends on the accuracy of the kinematic model used to describe its geometric structure. Manufacturing errors in the machining and assembling of manipulators leads to differences between the model parameters and the real physical configuration of the robot, causing positioning errors. In order to improve kinematic performance the actual parameters of a robot manipulator have to be identified.

Robot calibration is the process of identifying and quantifying various factors which contribute to positioning errors. Robot calibration can be divided into two levels [Kazerounian and Qian 1990]. The first level is the *Kinematic calibration*, which is the process of estimating errors in the parameters of the kinematic model of the robot. The second level is *Dynamic Calibration*, which involves errors in inertial properties of the robot links. Robot kinematic calibration usually involves two steps [Renders et al. 1991]:

- *Modeling*: Obtaining a kinematic model for the manipulator.
- *Identification and Correction*: Identifying parameters that affect positioning accuracies and compensating for the errors detected.

There are mainly two types of errors - *internal errors* and *external errors* - which affect positioning accuracy [Ishii et al. 1987]. Errors which are characteristic of the robot are described as internal errors. These can be further classified as *geometric* and *non-geometric* errors. The *geometric* errors are due to the errors in the geometric link parameters and joint readings. The important sources of geometric errors are:

- *length of links*: errors in lengths of the robot links.
- *position and angle variations at the joints*: for example, parallel joints may not be manufactured as perfectly parallel but with slight deviations.
- *offset errors at joint encoders*: electrical zeroes of the encoders may not coincide with mechanical zeroes of the joints.

The *non-geometric* errors result from friction, gravity and gear backlash. The external errors are the ones which arise due to inaccuracies in robot installation. They usually relate to position and orientation of the robot base in terms of world coordinates. These errors have to be taken into account when the robot is integrated with other equipment such as other robot systems. The process of identifying the internal errors is termed as *Robot internal calibration* and that of external errors as *Robot external calibration*. Once a robot has been calibrated internally, it need not be recalibrated when it is moved or reinstalled at a new location, as these parameters are specific to the robot, whereas the external calibration has to be carried out whenever the robot is reinstalled.

1.2.1 Robot Kinematic Models

Robot manipulators are made up of a number of links connected serially by actuated joints. For an n degree of freedom manipulator, there are n joints and n links. The base of the manipulator is link 0 and is not considered one of the n links. Link 1 is connected to link 0 by joint 1. The last link has a free end. The joints can be either revolute or prismatic. A robot *kinematic model* gives the relationship between the displacement at each joint and the end-effector position and orientation. In a kinematic model three dimensional coordinate frames are assigned to each link.

A stable kinematic model has sufficient parameters to represent all robot movements. Small changes in the physical structure of the robot manipulator should be reflected as small changes in the parameters [Zeigert and Datseris 1988]. The trans-

formation between two 3D coordinate frames is usually described by three rotational and three translational parameters. However, most kinematic models use less than six parameters for simplicity and certain restrictions are imposed such as where to place the origin of the coordinate system and so on.

Various models have been developed by researchers in the past. Most of these models include only the geometric parameters and ignore the non-geometric ones. Due to the complexity involved, the non-geometric aspects such as gear friction and backlash are not included in the kinematic models. Also, since different mechanisms are used in the design of manipulators, it is difficult to create a general model to describe the non-geometric effects. Some researchers have developed non-geometric models to predict and compensate for non-geometric errors [Ahmad 1988]. These models are more complicated and difficult to implement and are developed independent from geometric models. Some models introduce additional parameters into the geometric model to compensate for the non-geometric errors [Caenen and Angue 1990, Whitney et al. 1984]. Figure 1.3 shows a kinematic model which compensates for both geometric and non-geometric errors. Some models generally used for calibration procedures are discussed below.

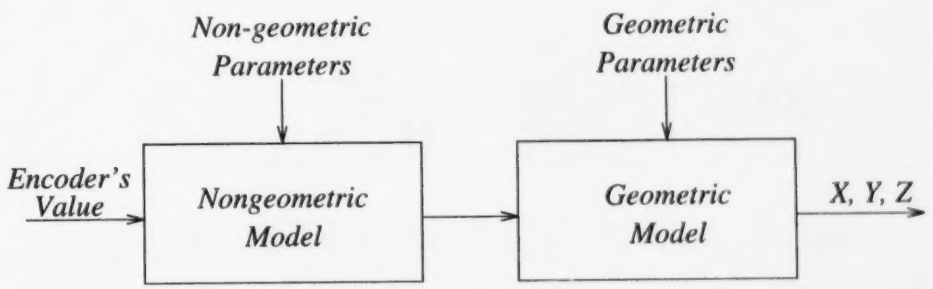

Figure 1.3: Robot Kinematic Model with Non-geometric Parameters.

The basic robot kinematic model is the *Denavit and Hartenberg, (D-H)* model. This model uses homogeneous transformation matrices known as A matrices to obtain relationships between two adjacent links. Thus for an n-link robot there are n A matrices (A_1,...A_n), and the position and orientation of the end-effector (T) with

respect to the base of the robot is given by,

$$T = A_1 A_2 .... A_n$$

This model uses four parameters to describe the link transformation A_i [McKerrow 1990]. Mathematically, the link transformation between two coordinate frames i and $i-1$ can be represented as a series of rotations – *Rot* and translations – *Trans*:

$$A_i = Rot(z, \theta_i) Trans(0, 0, d_i) Trans(l_i, 0, 0) Rot(x, \alpha_i)$$

Thus the D-H model of a n-link manipulator has $4n$ parameters. The four link parameters are defined as follows:

- l_i: is the link length.
- α_i: is the link twist.
- d_i: the distance between the links.
- θ_i: the angle between links.

Figure 1.4 shows the definition of these parameters for a revolute joint [Stone 1987]. l_i is the length of the common normal between the joint i and joint $i+1$ axes (z_{i-1} and z_i). α_i is the angle that exists between the joint axes if the origins of the joint frames coincide. θ_i is the angle between the common normals of successive links (x_{i-1} and x_i). d_i is the distance along the axis of the joint (z_{i-1}) between the intersection of the common normals of the adjacent links with the joint axes. The link parameter which can be varied is known as the joint variable. For a revolute joint, θ_i is the joint variable whereas for a prismatic joint, d_i is the joint variable. Some features of the D-H model are [Stone 1987]:

- The z_{i-1} axis is aligned with the joint axis.
- The x_{i-1} axis is parallel to the common normal.
- The coordinate origins on the links are at the intersection of the common normal between the joint $i-1$ and joint i axes with the joint i axis.

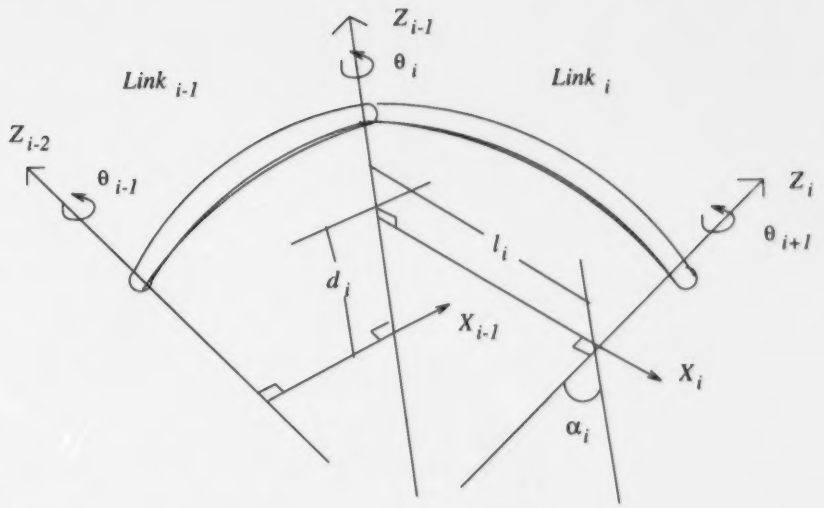

Figure 1.4: The *D-H* Kinematic Model: Four Parameters.

Though this model is simple, it has some drawbacks. First, when the adjacent joint axes are parallel, the common normals are no longer unique which makes the parameter d_i indefinite. Second, it is difficult to manufacture exactly parallel axes, and any slight deviations would cause the length of the common normal to vary and would also move the coordinate origin to different locations [Ishii 1991]. This violates the assumptions for a stable calibration model which requires that any small changes in the structure correspond to small changes in the model parameters.

Several researchers have modified the basic D-H model to overcome this difficulty by introducing extra parameters into the model. Hayati developed a model which uses five parameters to describe link transformations [Hayati and Mirmirani 1985, Hayati et al. 1988]. A new rotational parameter β_i is introduced into the model. This extra parameter defines the rotation of a frame i to a new frame i' around the Y axis for non-exactly parallel joints. This selection of parameters allows small errors between two joint coordinate frames to be modeled as small errors in the parameters. This prevents rapid changes in parameter d_i which is a problem in the D-H model. Figure 1.5 shows the parameters of the modified D-H model. The link transformation

can be represented as follows:

$$A_i = Rot(z,\theta_i)Trans(0,0,d_i)Trans(l_i,0,0)Rot(x,\alpha_i)Rot(y,\beta_i)$$

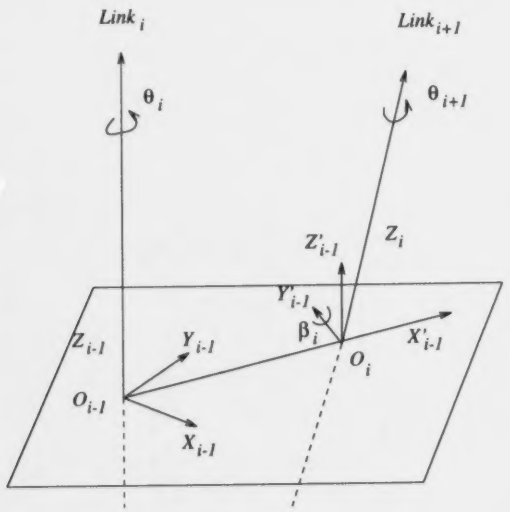

Figure 1.5: The *Hayati* Kinematic Model: Five Parameters.

Whitney and Lozinski [Whitney et al. 1984] developed a model which contains both geometric and non-geometric components. The geometric component consists of six parameters. The link transformation can be represented as follows:

$$A_i = Rot(y,\theta_i)Trans(0,y_i,z_i)Rot(x,\alpha_i)Rot(y,\beta_i)Rot(z,\phi_i)$$

The last three terms refer to roll-pitch-yaw rotational transformations. For a revolute joint θ_i is the joint variable and y_i is the variable for a prismatic joint. Thus for a n-link robot the model has $6n$ geometric parameters. Some features of this model are:

- The y axis of the link frame is along the joint axis.
- The origin of the coordinate frame must lie on the joint axis.

With the two additional parameters for each link transformation there is greater flexibility is assigning locations of the coordinate frames. As a result, the model is more complex than the D-H model.

Stone and Sanderson [Stone 1987] have developed a kinematic model (*S-model*) which has six parameters. The link transformation can be represented as follows:

$$A_i = Rot(z,\theta_i)Trans(0,0,d_i)Trans(l_i,0,0)Rot(x,\alpha_i)Rot(z,\phi_i)Trans(0,0,b_i)$$

For an n-link robot manipulator, $6n$ parameters are required to specify the S-model of the robot. Since each transformation is specified by six parameters rather than four, the S-model is less restrictive than the D-H model in locating the coordinate frames. Some features of the S-model which are equivalent to the D-H model are:

- The z axis of the coordinate frame is parallel to the joint axis.
- The origin of the frame must lie on the joint i axis.

An important difference between the S-model and the D-H model link frames is that the origin of the frame is not fixed but arbitrary. Figure 1.6 shows the S-model frames and the D-H model link frames. The angle ϕ_i is defined as the angular displacement between the x axes of the D-H frame (T_i) and the S-model coordinate frame (S_i). The parameter b_i is the linear displacement between the origins of T_i and S_i. For a revolute joint, θ_i is the joint variable whereas for a prismatic joint, d_i is the variable.

The accuracy of a kinematic model depends on the various assumptions made during its development. In order to improve the positioning accuracy of the robot manipulator it is necessary to find the values of the model parameters which best represent the robot structure.

1.3 Thesis Outline

Chapter 1 presented the problems of camera and robot calibration and their importance in the field of robotics and vision. A few mathematical models for both the camera and robot manipulator were described. The remainder of the thesis is orga-

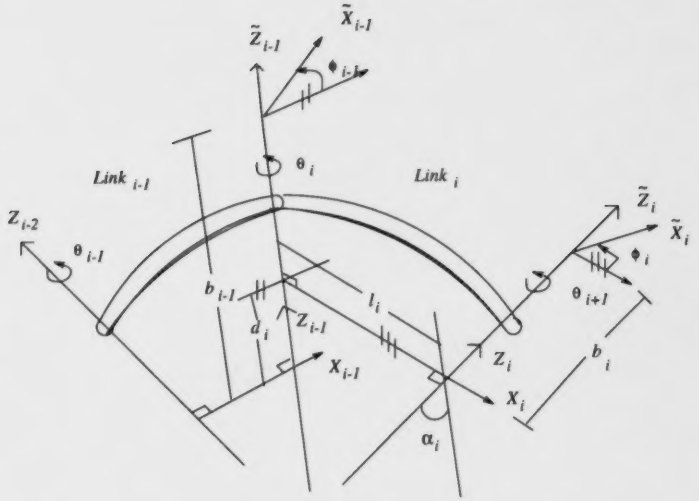

Figure 1.6: The *S-Model*: Six Parameters.

nized as follows. Chapter 2 briefly describes previous research in camera and robot manipulator calibrations. Various calibration techniques are discussed.

Chapter 3 presents a novel internal camera calibration technique, the active camera calibration. Algorithms are presented for the calibration of internal parameters (focal length and image center). Mathematical derivations and proofs are also provided. Chapter 4 presents a kinematic calibration procedure for a robot manipulator. The basic setup and procedure of the calibration technique are presented along with the mathematical equations.

Chapter 5 provides some experimental results of the calibration techniques presented in chapters 3 and 4. Results of simulation and real experiments are provided for the camera calibration techniques. Simulation results are provided for the robot kinematic calibration technique. A three-link robot manipulator is considered for the simulations. Chapter 6 presents some conclusions of this work and discusses directions for future research.

Chapter 2

Previous Work

This chapter presents various calibration techniques developed by researchers for both camera and robot manipulator. Camera calibration techniques are presented first, followed by robot calibration techniques.

2.1 Camera Calibration

Various camera calibration techniques have been developed by researchers in the past. These techniques can be broadly classified as *linear* and *non-linear* techniques and those which model lens distortions and those which do not. The techniques can also be classified according to the model used — *pin-hole* model or *two-plane* model. Some of the techniques are presented below.

2.1.1 Pin-hole Model

In this section, the calibration procedures which use the pin-hole camera model are discussed.

2.1.2 Non-linear Techniques

The transformation from 3D world points to image coordinates is a non-linear model consisting of the extrinsic parameters and the camera internal parameters (focal length, lens distortion, etc.). Many techniques have been developed which solve for the unknown parameters by performing non-linear optimizations from a set of equations obtained with known 3D points and their corresponding image points.

Faig [1975]'s technique is based on the pin-hole model. A very elaborate model is used which has upto seventeen unknowns. These unknowns are solved by a set of non-linear equations. The model is accurate due to the large number of parameters, but the technique is computer intensive and time-consuming. Also an initial guess for the model parameters is required to perform non-linear optimizations.

Wong [1975] presents a technique which solves for the model parameters using a set of linear equations if lens distortions are not considered. He shows that the system becomes non-linear if distortions are included in the model.

Sobel [1974] introduced a calibration technique which involves solving a large system of non-linear equations. Both intrinsic and extrinsic parameters are included in the model. The model had a total of eighteen parameters. This method also requires an initial guess. No accuracy results are reported.

Brown [1971] developed a technique which considers mainly the lens distortions. He pointed out that the distortions are not the same throughout the image, but vary according to the distortion model developed. A test field consisting of a series of plumb lines was used. Due to distortions the images of these lines were not straight. The distortion factors were estimated by attempting to correct the image points to conform to straight lines. Some experimental results are provided.

The techniques developed in [Gennery 1979, Okamoto 1981] are similar in that the parameters are solved iteratively until the values converge by using full-scale non-linear search.

The advantage of the non-linear techniques discussed above is that complex imaging models can be used; as a result the accuracy is increased. These methods have certain drawbacks such as: (1) an initial guess for the parameters is required to start the non-linear search; and (2) the techniques are computationally intensive and time-consuming.

2.1.3 Linear and Partially Linear Techniques

Although the transformation equations from the 3D world to 2D image points are non-linear functions of extrinsic and intrinsic camera parameters, they are linear if lens distortion is ignored and the coefficients of the transformation matrix are considered unknowns. Thus, given a number of known 3D points and their image points the coefficients of the transformation matrix can be solved by a least-squares solution of the resulting linear equations. The model parameters can be obtained from these coefficients if needed.

Sutherland [1974], Hall et al. [1982] formulated methods to obtain the transformation matrix given a set of 3D points and their known image points. No experimental and accuracy results are reported.

Ganapathy [1984] derived a non-iterative technique to obtain the camera parameters from a given perspective matrix. The transformation matrix, conversion from 3D to 2D image points, is represented as a series of operations. Lens distortion is not considered. The camera's extrinsic and intrinsic parameters are then obtained by a non-iterative method. Strat [1984] developed a similar technique to obtain the camera parameters from a known transformation matrix using simple geometric characteristics.

Yakimovsky and Cunningham [1978] presented a linear calibration technique. Lens distortion was not considered. Also, some combinations of the model parameters were considered as single variables in order to formulate the problem as a system of

linear equations, although the variables may not be completely linearly independent. This may limit the accuracy of the model in noisy situations.

Tsai [1987] developed a two-stage partially linear technique which involves only radial distortion. The calibration procedure is divided into two stages. In the first stage, most of the extrinsic parameters, the rotational elements and two translational elements are calibrated. The computations are simple, as the relationships between these parameters can be transformed into linear ones. In the second stage, the other extrinsic and intrinsic parameters are computed using the values computed in the first stage. The equations in the second stage are simple and non-linear. In this method, it is assumed that the image center is known *a priori*. In Tsai and Lenz [1988] a technique for estimating the image center is presented. Chang and Liang [1989] reformulated Tsai's method so that a two-stage Kalman filter can be used to solve for the camera parameters recursively. William and Louis [1987] also presented a method based on Tsai's two stage technique.

Beardsley et al. [1992] presented a technique which uses vanishing points. Only intrinsic parameters are considered. No lens distortions are considered. The system consists of a static camera which takes a sequence of images of a calibration plane rotating around a fixed axis. For each image the vanishing points, and hence the vanishing line, are determined. As the calibration plane moves, the vanishing points move along a conic envelope. A method is described as to how these conic sections can be used to determine the camera parameters. Multiple images are used to reduce the noise effect. Wei et al. [1989] also presented a method based on vanishing point geometry. In this method lens distortions are considered.

Faugeras et al. [1992] presented a technique which uses a camera in motion (only translation) to calibrate for the internal parameters. The motion of the camera need not be known and no calibration object is required. The method requires point-to-point matches between the image sequences. Horaud et al. [1992], Bani-Hashemi [1992], Faugeras and Toscani [1986] also presented linear techniques for calibration of

the camera parameters.

The linear techniques are simpler and computationally less expensive. No non-linear optimization is needed. But most of the linear techniques do not consider lens distortions.

2.1.4 Two-plane Model

In this section, calibration techniques which use the two-plane camera model are presented.

Martins et al. [1981] uses the two-plane model for camera calibration. The system of equations obtained is fully linear and does not involve any non-linear operations. Data from two calibration planes is used to predict the locations of 3D points of corresponding image points by interpolation. The performance of various interpolation techniques is discussed. This method assumes that the two calibration planes are parallel, and only backward computation is possible.

Gremban et al. [1988] also used the two-plane model. They developed a calibration procedure to solve both the forward and backward projections. Various interpolation strategies were tested and the accuracy results given. The effect of the number of calibration points used on the planes was also studied.

Izaguirre et al. [1985] extended the two-plane method to include the position and orientation of the camera. They used an iterative approach based on Kalman-filters for solving the equations. Wei and Ma [1991] also presented a technique based on the two-plane model, similar to Martin's, but in this method the planes need not be parallel to each other. The calibration technique developed in [Champleboux et al. 1992] also uses the two-plane model.

2.2 Robot Calibration

Various robot calibration techniques have been developed in the past. The techniques differ in the kinematic model used for calibration, some include both geometric and non-geometric errors, and the sensors used to aid the calibration. A general solution which is used in most of the techniques is presented first, followed by some calibration techniques.

2.2.1 General Solution

The derivation of robot parameters is usually done using the following procedure. If the model consists of n kinematic parameters $(Q_1, Q_2, \ldots, Q_n)$, the relationship between the end-effector position and orientation vector $\mathbf{x}$ and the parameters is given by:

$$\mathbf{x} = f(Q_1, Q_2, \ldots, Q_n)$$

This relation is non-linear in the geometrical parameters. For example, for a five parameter model,

$$\mathbf{x} = f(\theta, \alpha, l, d, \beta) = f(\phi)$$

where θ, α, l, d, and β are n-length vectors for an n-joint robot. The variation in $\mathbf{x}$, $\Delta\mathbf{x}$ can be obtained as a function of variations in the parameters, $\Delta\phi = (\Delta\theta, \Delta\alpha, \Delta l, \Delta d, \Delta\beta)$ in the following way.

$$\begin{aligned} \Delta\mathbf{x} &= \frac{\partial f}{\partial\theta}\Delta\theta + \frac{\partial f}{\partial\alpha}\Delta\alpha + \frac{\partial f}{\partial a}\Delta l + \frac{\partial f}{\partial d}\Delta d + \frac{\partial f}{\partial\beta}\Delta\beta \\ &= J_\theta\Delta\theta + J_\alpha\Delta\alpha + J_a\Delta l + J_d\Delta d + J_\beta\Delta\beta \end{aligned}$$

where $J_\theta = \frac{\partial f}{\partial\theta}$, $J_\alpha = \frac{\partial f}{\partial\alpha}$, etc, are the Jacobians that reflect the sensitivity of the end-effector orientation and position with respect to the particular parameter [Renders et al. 1991].

A number of manipulator poses and measurements are required to determine these parameters. After rotating each axis m times and obtaining the error vector $\Delta \mathbf{x}_i$, the following equation can be obtained,

$$\begin{pmatrix} \Delta \mathbf{x}_1 \\ \Delta \mathbf{x}_2 \\ \vdots \\ \Delta \mathbf{x}_m \end{pmatrix} = \begin{pmatrix} C_1 \\ C_2 \\ \vdots \\ C_m \end{pmatrix} \Delta\phi \Longrightarrow b = D\Delta\phi$$

The least squares solution for $\Delta\phi$ is obtained as,

$$\Delta\phi = (D^T D)^{-1} D^T b$$

The updated values of the parameters are obtained as

$$\phi' = \phi + \Delta\phi$$

As this is a non-linear estimation problem, the procedure is iterated until the variations in $\Delta\phi$ approach zero and the values of the parameters converge. In each iteration, the new Jacobian is evaluated with the new parameters and used in the error equation [Hollerbach and Bennett 1988]. An initial estimate of the parameters is required.

The difference or error vector $\Delta\mathbf{x}$ in the orientation and position of the end-effector is obtained by measuring the difference in the measured endpoint location (or a reference point on the end link) $\mathbf{x}_m$, measured by means of a sensor, and the computed location of end-effector $\mathbf{x}_c$ from the model of the robot arm. Thus,

$$\Delta\mathbf{x} = \mathbf{x}_m - \mathbf{x}_c$$

Most techniques use this procedure to find the errors in the model parameters. Measurement of the end-effector (reference point) is an important problem in robot calibration. Many methods have been developed which use different sources for this measurement. Some of them are discussed below.

2.2.2 Calibration Techniques

Vietschegger and Wu [1988] developed a method which uses the five-parameter Hayati model discussed in chapter 1. Only geometric parameters are included in the model. As well, only four parameters are allowed to vary. For example, in the case of parallel axes, the parameter β_i is allowed to vary and d_i is assumed to be error-free. For calibration purposes, a tool is mounted on the end-effector to detect contact between the end-effector and a specially fabricated high precision plate with known points in the world coordinate frame. Only the position of the reference point is obtained. The end-effector is moved to different positions and the error values are found by solving a system of equations using a least squares approach. Experiments were performed on the PUMA 560 robot.

Renders et al. [1991] developed a technique to determine both geometric and non-geometric errors. The errors in position and orientation of the measuring device are included in the calibration algorithm to be identified. Hollerbach and Bennett [1988] presented a technique to estimate the geometric errors. The five parameter kinematic model was used. These two techniques use an infrared three dimensional measurement system for the calibration. These measuring systems are based on a stereoscopic analysis by two cameras of the location of a light emitting diode (IRED) fixed on the end-effector. Three IREDS are used to find the position and orientation of the frame attached to the end-effector. These systems are sensitive to reflections.

Whitney et al. [1984] developed a calibration algorithm to identify both geometric and non-geometric parameters. A theodolite was used to measure the end-effector position. Additional parameters were introduced into the robot model in order to relate the position of the end-effector to the angular coordinates of the theodolite. A non-linear search procedure was used to solve for the parameters. Caenen and Angue [1990] developed a similar technique. Chen and Chao [1986] developed a method which used three theodolites to obtain the position and orientation of the end-effector. Both geometric and non-geometric parameters were identified. Driels

and Uday [1991] used a similar method but instead of theodolites, a vision system was used to track an illuminated target mounted on the end-effector. These measurements provide good accuracy but are time consuming when performing automatic tracking.

Stone [1987] used a six parameter model (S-Model), discussed in chapter 1, to identify the geometric parameters. An external ultrasonic range sensor was used to find the position of the target points attached to each of the links. Thus in this method each link is calibrated independently by moving one link at a time through its range.

Similar calibration techniques are presented in [Borm and H. 1989, Kazerounian and Qian 1990, Judd and Knasinski 1987, Zak et al. 1993]. An overview of various measurement techniques used for robot calibration is presented in [Nowrouzi et al. 1988].

Puskorius and Feldkamp [1987] developed a technique which uses a vision system to calibrate the robot manipulator. The robot/vision system is calibrated simultaneously. The method employs a stereo-pair of cameras mounted rigidly on the end-effector. The image points of a target point in space are obtained by the stereo-pair for different joint configurations. Both geometric and non-geometric parameters of the robot model, as well as the vision system parameters, are obtained by an iterative least-squares algorithm. Some experimental results are provided. David et al. [1991] also presented a similar approach, but the stereo-pair was used as an external sensor, i.e, the stereo-pair was not mounted on the robot arm, and used to track a point on the robot end-effector. Only geometric parameters were identified. Both these techniques used the five-parameter robot kinematic model.

Preising and Hsai [1991] developed a technique to measure the accuracy and repeatability of a robot manipulator. A single camera was used to track a point on the end-effector. Roth et al. [1987] also developed a technique which uses a single passive camera. The camera is mounted on the robot manipulator and image of a calibration object with known 3D points is captured. The robot geometric parameters are

calibrated along with the camera parameters. All transformations from robot base to world frame, end-effector frame to camera frame are included in the calibration algorithm. An initial estimate of all the parameters is required.

Lenz and Tsai [1989] presented a calibration technique using a camera mounted on the robot manipulator. The calibration technique is performed by moving only one joint at a time and obtaining the resulting motion in the camera, with the view fixed on a calibration object with known 3D points in the world frame. The joint axis of rotation and angle of rotation relative to the world frame are found. No attempt is made to obtain the geometric parameters of the kinematic model.

2.3 Conclusions

This chapter presented some of the calibration techniques for camera and robot manipulator. Most of the camera calibration techniques use a static camera and a known 3D pattern. Although non-linear techniques are accurate due to the elaborate model, they are computationally expensive and require an initial guess for the parameters. Linear techniques are simpler but most of them do not account for lens distortions. Robot calibration techniques require measurement system to estimate the position of the end-effector due to different joint positions. Various measurement systems have been used to estimate the position of the end-effector. Some of the experimental setups are elaborate and expensive. Systems have been developed which use cameras for performing the calibration and to aid hand-eye coordination. Some techniques use the vision system as an external sensor with the camera mounted separately, and some use the camera mounted on the robot manipulator. These techniques usually have a lower accuracy compared to other devices; their accuracy is limited by the accuracy of camera measurements and camera resolution.

Chapter 3

Active Camera Calibration

In this chapter novel techniques to calibrate the *internal parameters* of the camera are presented. It is shown that an active camera capable of *rotational movements* can automatically calibrate itself.

3.1 Introduction

Most of the existing camera calibration techniques [Tsai 1987, Brown 1971, Sobel 1974] discussed in chapter 2, use a known calibration pattern and a static camera. A set of known calibration points is used and their image projections are related to the camera parameters. Most of the techniques perform external and internal calibration together, as a single process, and require point-to-point matching. As *active vision* systems and algorithms [Aloimonos et al. 1987] become more popular, it is necessary to develop calibration techniques for active cameras. An *active visual* system is defined as one which is able to manipulate its parameters in order to extract useful data from the scene being viewed [Aloimonos 1993]. Active systems have many applications such as tracking of moving objects, navigation, etc. In addition, problems such as determining shape from contours and depth perception are easier

to solve with active vision techniques [Aloimonos et al. 1987]. Since in active vision systems the camera's paramters (such as focal length) may change, it is necessary to calibrate for the internal parameters automatically and efficiently, without the use of any predefined patterns. The process of determining the parameters of the camera model by moving the camera is termed as *active camera calibration.*

When a camera rotates, new image points can be obtained as a transformation of the original image points [Kanatani 1987]. The camera parameters can be related to the image points before and after rotation and to the angle of rotation. Equations describing these relations are simple and easy to solve. Thus by considering different movements of the camera (pan, tilt and roll), the internal parameters (focal length and image center) of the camera can be estimated. In this thesis, only the focal length and image center are considered. Although there are various possible definitions of image center, the coordinates of which differ from each other for a real lens [Wilson and Shafer 1993], the image center considered in this thesis is the intersection of the optical axis with the image plane. Lens distortion is ignored, as lenses which correct for distortions are easily available.

The calibration procedure developed for determining the internal parameters of the camera in [Basu 1993] is an active calibration technique which does not require any pre-defined patterns — unlike various other existing calibration techniques [Horaud et al. 1992, Bani-Hashemi 1992]. No initial estimates of the focal length are required, a reasonable estimate of the lens center is sufficient. This technique uses a set of stable edges and some simple computations to determine the focal length and image center. The algorithms introduced in [Basu 1993] consider only pan and tilt movements of the camera and the equations for computing the image center are sensitive to noise. These algorithms are extended to consider roll movements of the camera to obtain a more robust and simple procedure for computing the image center. The two algorithms (Strategy A and Strategy B) developed in [Basu 1993] are presented along with the new techniques developed.

3.2 Mathematical Derivations

In this section, lemmas and propositions required for the calibration techniques are presented. Consider the pin-hole camera model with perspective projection shown in Figure 3.7. The following notations are used throughout this chapter.

- (x,y): The image coordinates.
- f_x: Focal length in pixels in the x direction.
- f_y: Focal length in pixels in the y direction.
- (δ_x,δ_y): Error in the estimated image center.
- $R = (r_{ij})_{3\times3}$: Rotation matrix.
- (X,Y,Z): Point in 3D world.
- (x_p,y_p): Image coordinates after pan movement.
- (x_t,y_t): Image coordinates after tilt movement.
- (x_r,y_r): Image coordinates after roll movement.
- θ_t: Tilt angle.
- θ_p: Pan angle.
- θ_r: Roll angle.
- $T = [\Delta X \Delta Y \Delta Z]^T$: Translation matrix

The following lemmas and propositions are developed assuming $\delta_x = \delta_y = 0$, no error in image center.

Lemma 3.1 *If the camera rotates by a rotation matrix R and translates by T relative to a static scene, the new image points (x_n,y_n) are related to the original points (x,y) as follows,*

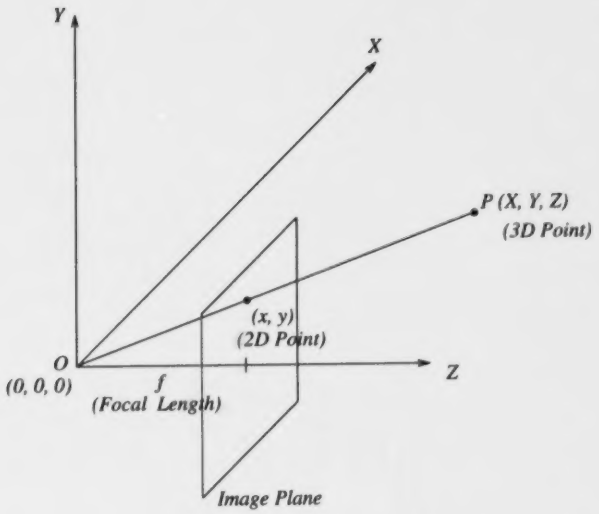

Figure 3.7: Camera Model: Perspective Projection.

$$x_n = \frac{r_{11}x + r_{21}\frac{f_x}{f_y}y + r_{31}f_x - f_x\frac{\Delta X}{Z}}{r_{13}\frac{x}{f_x} + r_{23}\frac{y}{f_y} + r_{33} - \frac{\Delta Z}{Z}} \tag{3.1}$$

$$y_n = \frac{r_{12}\frac{f_y}{f_x}x + r_{22}y + r_{32}f_y - f_y\frac{\Delta Y}{Z}}{r_{13}\frac{x}{f_x} + r_{23}\frac{y}{f_y} + r_{33} - \frac{\Delta Z}{Z}} \tag{3.2}$$

Proof:

It follows from the fact that rotation (translation) of the camera is equivalent to inverse rotation (translation) of the 3D points. Thus,

$$\begin{bmatrix} X_n \\ Y_n \\ Z_n \end{bmatrix} = \begin{bmatrix} r_{11} & r_{21} & r_{31} \\ r_{12} & r_{22} & r_{32} \\ r_{13} & r_{23} & r_{33} \end{bmatrix} \begin{bmatrix} X \\ Y \\ Z \end{bmatrix} - \begin{bmatrix} \Delta X \\ \Delta Y \\ \Delta Z \end{bmatrix}$$

and by the perspective projection,

$$x_n = f_x\frac{X_n}{Z_n}$$
$$y_n = f_y\frac{Y_n}{Z_n}$$

where,

- (X, Y, Z): Original 3D point.

- (X_n, Y_n, Z_n): New 3D point.
- (x_n, y_n): New image point.

Proposition 3.1 *If the camera tilts (rotates about the X-axis) by a small angle θ_t and the depth (Z) is large compared to ΔX, ΔY, ΔZ:*

$$x_t \cong x(1 + \theta_t \frac{y}{f_y}) \tag{3.3}$$

$$y_t \cong (y + \theta_t f_y)(1 + \theta_t \frac{y}{f_y}) \tag{3.4}$$

Similarly, for a small pan angle θ_p (rotation about Y-axis),

$$x_p \cong (x - \theta_p f_x)(1 - \theta_p \frac{x}{f_x}) \tag{3.5}$$

$$y_p \cong y(1 - \theta_p \frac{x}{f_x}) \tag{3.6}$$

Proofs:

For a small pan angle (θ_p), the rotation matrix (R_p) can be approximated as

$$\begin{pmatrix} 1 & 0 & \theta_p \\ 0 & 1 & 0 \\ -\theta_p & 0 & 1 \end{pmatrix}$$

By substituting into equations (3.1) and (3.2) and neglecting $\frac{\Delta X}{Z}$, $\frac{\Delta Y}{Z}$, and $\frac{\Delta Z}{Z}$ the following equations are obtained:

$$x_p \cong (x + \theta_p f_x)(1 + \theta_p \frac{x}{f_x})^{-1}$$

$$y_p \cong y(1 + \theta_p \frac{x}{f_x})^{-1}$$

Since θ_t is small, the R.H.S of the equations can be expanded using the Taylor series, and higher order terms can be ignored to get the equations (3.5) and (3.6).

For a small tilt angle (θ_t), the rotation matrix (R_t) can be approximated as

$$\begin{pmatrix} 1 & 0 & 0 \\ 0 & 1 & -\theta_t \\ 0 & \theta_t & 1 \end{pmatrix}$$

Following the same procedure as for pan movement, the equations (3.3) and (3.4) are obtained.

Proposition 3.2 *If the camera rolls (rotation about the Z axis) by an angle θ_r then,*

$$x_r = \cos(\theta_r)x + \sin(\theta_r)\frac{f_x}{f_y}y \tag{3.7}$$

$$y_r = -\sin(\theta_r)\frac{f_y}{f_x}x + \cos(\theta_r)y \tag{3.8}$$

Proof:

The rotation matrix (R_r) for rotation about the Z axis (roll movement) is as follows:

$$\begin{pmatrix} \cos(\theta_r) & -\sin(\theta_r) & 0 \\ \sin(\theta_r) & \cos(\theta_r) & 0 \\ 0 & 0 & 1 \end{pmatrix}$$

Assuming that ΔX, ΔY and ΔZ are small compared to depth Z, which makes the terms $\frac{\Delta X}{Z}$, $\frac{\Delta Y}{Z}$ and $\frac{\Delta Z}{Z}$ negligible, and using the relations in Lemma (3.1) equations (3.7) and (3.8) are obtained. It is assumed that the axis of rotation is coincident with the camera z axis.

3.3 Strategies for Active Calibration

Using the geometric relations presented in section 3.2, the camera parameters can be obtained given some information of stable image contours before and after the camera motions and contour-to-contour correspondence between the images and angle

of pan/tilt/roll. Since most current active cameras are equipped with potentiometers, estimates of angles can be obtained from the potentiometer readings. Figure 3.8 shows the schematics of such a device. In this section it is shown that by small pan/tilt and roll movements, an active camera can obtain estimates of the focal length and image center by solving a simple system of linear equations. A few propositions as well as the active calibration procedures are developed.

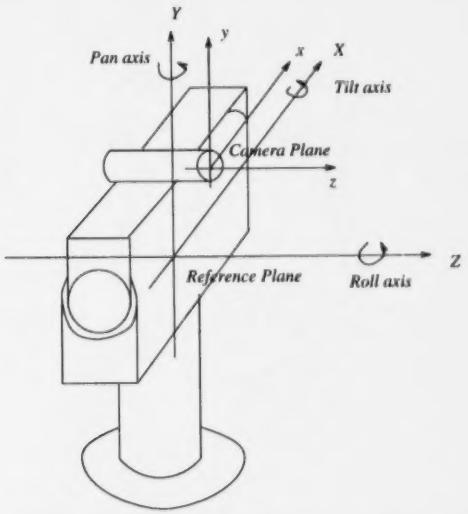

Figure 3.8: Schematics of an Active Camera.

Proposition 3.3 *If the center of the lens is estimated with a small error* $(\delta x, \delta y)$ *then* f_x *and* f_y *can be approximated as follows:*

$$f_x \cong \frac{-\theta_p}{(\overline{y_p} - \overline{y})}(\overline{xy} - \overline{x}\delta_y - \overline{y}\delta_x) \tag{3.9}$$

$$f_y \cong \frac{\theta_t}{(\overline{x_t} - \overline{x})}(\overline{xy} - \overline{x}\delta_y - \overline{y}\delta_x) \tag{3.10}$$

where "$-$" represents the average taken over an image contour.

Proof:

By replacing x by $x - \delta_x$ and y by $y - \delta_y$ in equations (3.3) and (3.6), and ignoring the term $\delta_x\delta_y$ (since the error is small and the angle is small), equations (3.9) and (3.10) are obtained.

Proposition 3.4 *Using tilt (or pan) movements and considering three independent contours two linear equations in δ_x and δ_y can be obtained as follows:*

$$\overline{x^{(2)}y^{(2)}} - K_1\overline{x^{(1)}y^{(1)}} = (\overline{x^{(2)}} - K_1\overline{x^{(1)}})\delta_y + (\overline{y^{(2)}} - K_1\overline{y^{(1)}})\delta_x \tag{3.11}$$

$$\overline{x^{(3)}y^{(3)}} - K_2\overline{x^{(1)}y^{(1)}} = (\overline{x^{(3)}} - K_2\bar{x^{(1)}})\delta_y + (\bar{y^{(3)}} - K_2\bar{y^{(1)}})\delta_x \tag{3.12}$$

where $K_1 = \frac{(\overline{x_t^{(2)}} - \overline{x^{(2)}})}{(\overline{x_t^{(1)}} - \overline{x^{(1)}})}$ and $K_2 = \frac{(\overline{x_t^{(3)}} - \overline{x^{(3)}})}{(\overline{x_t^{(1)}} - \overline{x^{(1)}})}$. The points $(x^{(1)}, y^{(1)})$, $(x^{(2)}, y^{(2)})$ and $(x^{(3)}, y^{(3)})$ denote points lying on the three contours respectively.

Proofs:

Let C_1, C_2 and C_3 be three different contours, and $(x^{(1)}, y^{(1)})$, $(x^{(2)}, y^{(2)})$ and $(x^{(3)}, y^{(3)})$ be the points lying on them. From Proposition (3.3),

$$f_y \cong \frac{\theta_t}{(\overline{x_t^{(1)}} - \overline{x^{(1)}})}(\overline{x^{(1)}y^{(1)}} - \overline{x^{(1)}}\delta_y - \overline{y^{(1)}}\delta_x) \tag{3.13}$$

$$f_y \cong \frac{\theta_t}{(\overline{x_t^{(2)}} - \overline{x^{(2)}})}(\overline{x^{(2)}y^{(2)}} - \overline{x^{(2)}}\delta_y - \overline{y^{(2)}}\delta_x) \tag{3.14}$$

$$f_y \cong \frac{\theta_t}{(\overline{x_t^{(3)}} - \overline{x^{(3)}})}(\overline{x^{(3)}y^{(3)}} - \overline{x^{(3)}}\delta_y - \overline{y^{(3)}}\delta_x) \tag{3.15}$$

Equating the R.H.S of equations (3.13) and (3.14), and equations (3.13) and (3.15), the two linear equations (3.11) and (3.12) are obtained.

Strategy A:

The calibration procedure can be outlined as follows,

- Using three image contours before and after the camera movements (tilt or pan), estimate the values of δ_x and δ_y by solving the two linear equations (3.11) and (3.12).
- Considering a single image contour and substituting the above estimates of δ_x and δ_y in equations (3.9) and (3.10), obtain estimates for f_x and f_y.

The major problem with this procedure is that the terms (x_t - x) and (y_p - y) are produced by the perspective distortions when the camera moves and these are very small (only a few pixels) for small angles. Thus in case of noise and inaccuracies in contour localizations the relative error in these terms can be large, giving rise to unreliable estimates of focal length.

3.3.1 Alternative Strategy

An alternate strategy developed to overcome the drawback of Strategy A, is presented below. Although not theoretically accurate, the equations developed are simple and more reliable.

Proposition 3.5 *Using a single image contour and small pan/tilt movements the following equations in f_x and f_y are obtained ignoring negligible terms,*

$$f_x^2 - f_x\left(\frac{\overline{x_p} - \overline{x}(1+\theta_p^2)}{-\theta_p}\right) + \overline{x^2} = 0 \tag{3.16}$$

$$f_y^2 - f_y\left(\frac{\overline{y_t} - \overline{y}(1+\theta_t^2)}{\theta_t}\right) + \overline{y^2} = 0 \tag{3.17}$$

Proof:

From equation (3.4) in Proposition (3.1), when δ_x and δ_y are non-zero,

$$(y_t - \delta_y) \cong (y - \delta_y + \theta_t f_y)\left(1 + \theta_t \frac{(y-\delta_y)}{f_y}\right)$$

After simplifications,

$$y_t - y\,(1+\theta_t{}^2) - \frac{\theta_t y^2}{f_y} \cong \theta_t f_y - \delta_y \theta_t{}^2 + \frac{\theta_t \delta_y{}^2}{f_y} - \frac{2\theta_t \delta_y y}{f_y}$$

Even if the values of δ_x and δ_y are as large as 50 pixels, the last three terms of the above equation are negligible, since θ_t is less than 0.05 radians and the focal length is approximately 900 pixels. Thus the simplified equation is

$$f_y \cong \frac{\overline{y_t} - \overline{y}(1+\theta_t{}^2)}{\theta_t} - \frac{\overline{y^2}}{f_y} \tag{3.18}$$

On simplifying equation (3.18), the equation (3.17) in f_y is obtained. Similarly, from equation (3.5) of proposition (3.1), the equation (3.16) in f_x is obtained.

Corollary 3.1 *Given two independent contours and camera pan/tilt movements, and estimates of f_x and f_y (f_x^e and f_y^e), δ_x and δ_y can be obtained by solving the following equations:*

$$f_y^e \frac{(\overline{x_t^{(1)}} - \overline{x^{(1)}})}{\theta_t} = (\overline{x^{(1)}y^{(1)}} - \overline{x^{(1)}}\delta_y - \overline{y^{(1)}}\delta_x) \tag{3.19}$$

$$f_y^e \frac{(\overline{x_t^{(2)}} - \overline{x^{(2)}})}{\theta_t} = (\overline{x^{(2)}y^{(2)}} - \overline{x^{(2)}}\delta_y - \overline{y^{(2)}}\delta_x) \tag{3.20}$$

Proof:

Follows from Proposition (3.3).

Practical Considerations

Consider equation (3.17). For most practical systems the absolute value of y is less than 300, whereas f_y is greater than 500. Thus the equation is of the form $Af_y^2 + Bf_y + C = 0$, with $A = 1$, B negative and C small, compared to B. Thus the feasible solution to this quadratic equation is

$$f_y = \frac{\overline{y_t} - \overline{y}(1+\theta_t^2)}{2\theta_t} + \frac{1}{2}\sqrt{\left(\frac{\overline{y}(1+\theta_t^2) - \overline{y_t^2}}{\theta_t}\right)^2 - 4\overline{y^2}} \tag{3.21}$$

The other root is close to zero and thus can be ignored. Similarly from equation (3.16), the solution for f_x is

$$f_x = \frac{\overline{x_p} - \overline{x}(1+\theta_p^2)}{-2\theta_p} + \frac{1}{2}\sqrt{\left(\frac{\overline{x}(1+\theta_p^2) - \overline{x_p^2}}{\theta_p}\right)^2 - 4\overline{x^2}} \tag{3.22}$$

Strategy B:

Thus the alternative active calibration procedure is as follows,

- Using a single image contour, obtain estimates for f_x and f_y from equations (3.21) and (3.22).

- Considering two image contours, estimates of δ_x and δ_y can be obtained from equations (3.19) and (3.20).

This strategy provides good estimates for focal lengths and the equations are obtained without the knowledge of the image center. However, the equations for computing the image center are unstable due to the presence of the terms $(x_t - x)$ and $(y_p - y)$ which, as mentioned before, are sensitive to noise. Thus roll movements of the camera have been considered to produce more stable equations to compute the image center.

3.3.2 Alternate Strategy for Computation of Image Center

Roll movements of the camera are considered in order to obtain a different technique for computing the image center. This technique overcomes the drawbacks of strategies A and B in that the equations for computing the image center are more robust to noise. The proposed techniques are stated below.

Proposition 3.6 *Using a single image contour and prior knowledge about the focal lengths f_x and f_y two linear equations can be developed in δ_x and δ_y by a roll movement of the camera.*

Proof:

Introducing δ_x and δ_y, the non-zero errors in the image center estimation, into equations (3.7) and (3.8), the following equations are obtained:

$$\overline{x_r} - \delta_x = \cos(\theta_r)(\overline{x} - \delta_x) + \sin(\theta_r)\frac{f_x}{f_y}(\overline{y} - \delta_y) \tag{3.23}$$

$$\overline{y_r} - \delta_y = -\sin(\theta_r)\frac{f_y}{f_x}(\overline{x} - \delta_x) + \cos(\theta_r)(\overline{y} - \delta_y) \tag{3.24}$$

By rearranging the equations,

$$\delta_x(1 - \cos(\theta_r)) + \delta_y(-\frac{f_x}{f_y}\sin(\theta_r)) = \overline{x_r} - \cos(\theta_r)\overline{x} - \frac{f_x}{f_y}\sin(\theta_r)\overline{y} \tag{3.25}$$

$$\delta_x(\frac{f_y}{f_x}\sin(\theta_r)) + \delta_y(1 - \cos(\theta_r)) = \overline{y}_r - \cos(\theta_r)\overline{y} + \frac{f_y}{f_x}\sin(\theta_r)\overline{x} \tag{3.26}$$

Strategy C:

Thus the procedure can be outlined as follows:

- Obtain the estimates of f_x and f_y using the procedure in Strategy B.
- Using a roll movement of the camera and a single image contour, obtain values of δ_x and δ_y from equations (3.25) and (3.26).

Corollary 3.2 *When the roll movement (angle) is equal to* 180 deg, *the values of* δ_x *and* δ_y *can be obtained directly using a single image contour.*

Proof:

When the roll angle θ_r is 180 deg the equations (3.23) and (3.24) reduce to

$$\overline{x_r} - \delta_x = -(\overline{x} - \delta_x) \Rightarrow \delta_x = (\overline{x_r} + \overline{x})/2 \tag{3.27}$$

$$\overline{y_r} - \delta_y = -(\overline{y} - \delta_y) \Rightarrow \delta_y = (\overline{y_r} + \overline{y})/2 \tag{3.28}$$

Strategy D:

The procedure can be outlined as follows:

- Considering a roll movement of 180 deg and a single image contour, obtain the estimates of δ_x and δ_y from equations (3.27) and (3.28).
- Obtain estimates of f_x and f_y from equations (3.16) and (3.17) along with the ignored terms in δ_x and δ_y (which have been determined in the above step).

The equations for focal length are theoretically more accurate than strategies A and B, which ignore negligible terms. Also, as the change in image coordinates will be greater at a larger angle, the relative error is smaller at $\theta_r = 180$ deg, compared to other roll angles. Thus the equations for computing the image center are also more stable.

Effect of roll angle on estimating δ_x and δ_y

The error in estimating the image center can be reduced by increasing the roll angle. Thus the error at $\theta_r = 180\,\text{deg}$ is less than at smaller angles.

By simplifying the two equations (3.25) and (3.26), it can be shown that the terms $(y_r - y)$ and $(x_r - x)$ are involved in estimating δ_x and δ_y. These terms are larger at larger angles (the distance between pixels before and after rotation) thus making the relative error smaller.

3.4 Theoretical Error Analysis

In this section we study the effects of various errors arising from different sources in the computation of focal length and image center by Strategy C.

Remark 3.1 *Error in measuring the pan/tilt angles generates a proportional error in the estimation of f_x and f_y.*

Proof: It can be seen from equation (3.16) that the estimation of f_x is proportional to the pan angle (θ_p), hence any error in this angle is reflected as an error in f_x. Similarly any error in the tilt angle (θ_t) results in a proportionate error in f_y.

Remark 3.2 *Error in measurements of the roll angle generates a proportional error in δ_x and δ_y.*

Proof: From equations (3.25) and (3.26) we can see that the values of δ_x and δ_y are dependent on the roll angle (θ_r), thus any error in this angle measurement will result in an error in estimating the image center.

Remark 3.3 *Error in the axis of roll will result in an error in computing the image center.*

Case 1 *If the axis of rotation (z') is parallel to the camera z axis (deviates from the sensor center by (dx,dy,dz)), then the error in estimating the image center is insignificant if the depth (Z) is large.*

Proof: Rotation about the axis z' is equivalent to the following three transformations:

- Translate the axis from (dx,dy,dz) to the origin of the sensor.
- Perform the actual rotation.
- Translate the center back to (dx,dy,dz).

Thus the resulting Rotation matrix would be

$$R = \begin{bmatrix} \cos\theta_r & \sin\theta_r & 0 & \cos\theta_r dx + \sin\theta_r dy - dx \\ -\sin\theta_r & \cos\theta_r & 0 & -\sin\theta_r dx + \cos\theta_r dy - dy \\ 0 & 0 & 1 & 0 \\ 0 & 0 & 0 & 1 \end{bmatrix}$$

and the errors in x_r (ϵ_x) and y_r (ϵ_y) would be

$$\epsilon_x \cong \frac{f_x}{Z}(\cos(\theta_r)dx + \sin(\theta_r)dy - dx)$$
$$\epsilon_y \cong \frac{f_y}{Z}(\sin(\theta_r)dx + \cos(\theta_r)dy - dy)$$

Since the errors in computing δ_x and δ_y are dependent on the errors in x_r and y_r, it can be seen from the above equations that if the depth (Z) is large compared to dx and dy, the error is not significant.

Case 2: *If the axis of rotation (z') is at an angle to the camera z axis, but lies in the yz plane, the error in estimating δ_x is not significant, whereas the error in δ_y is quite large.*

Proof: Rotation about the axis z' is equivalent to the following three transformations:

- Rotate the axis so that it coincides with z axis.
- Perform the actual rotation.

- Rotate the axis back to original.

Assuming that the error angle (θ_e) is small (so that $\cos(\theta_e) \cong 1$ and $\sin(\theta_e) \cong \theta_e$)), the resulting rotation matrix is

$$R = \begin{bmatrix} \cos\theta_r & \sin\theta_r & -\sin(\theta_r)\theta_e \\ -\sin\theta_r & \cos\theta_r & -\cos(\theta_r)\theta_e + \theta_e \\ \theta_e \sin(\theta_r) & -\theta_e \cos(\theta_r) + \theta_e & 1 \end{bmatrix}$$

Thus the errors in x_r (ϵ_x) and y_r (ϵ_y) would be (again assuming Z is large),

$$\epsilon_x \cong f_x \sin(\theta_r)\theta_e)$$

$$\epsilon_y \cong f_y\theta_e(1 - \cos(\theta_r))$$

From equations (3.25) and (3.26), by introducing the error terms ϵ_x and ϵ_y the errors in computing δ_x (e_x) and δ_y (e_y) are

$$e_x = \frac{\epsilon_x(1 - \cos(\theta_r)) - \epsilon_y(-\frac{f_x}{f_y}\sin(\theta_r))}{(1 - \cos(\theta_r)^2) + (\sin(\theta_r))^2}$$

$$e_y = \frac{\epsilon_y(1 - \cos(\theta_r)) - \epsilon_x(\frac{f_x}{f_y}\sin(\theta_r))}{(1 - \cos(\theta_r)^2) + (\sin(\theta_r))^2}$$

On simplification of the above two equations, the error in δ_x (e_x) $\cong 0$ and error in δ_y (e_y) $\cong f_y\theta_e$. Thus the error in δ_y is proportional to the error angle whereas the error in δ_x is insignificant.

Case 3: *If the axis of rotation z' lies in the xz plane, the error in δ_x is proportional to the error angle, whereas the error in δ_y is small.*

Proof: Similar to case 2.

Thus any error in the axis of rotation has a considerable effect on the estimation of the image center.

Remark 3.4 *The coefficients of the linear equations used for solving the image center ((3.25) and (3.26)) and the focal length ((3.21) and (3.22)) are unbiased in the presence of uncorrelated noise with zero mean.*

Proof (outline): The coefficients involve a linear combination of terms of the form: $\overline{x}$, $\overline{y}$. These terms are unbiased in the presence of uncorrelated noise with zero mean. Thus any linear combination of terms like the above is also unbiased [Basu 1993].

3.5 Conclusions

In this chapter, active calibration techniques which calibrate the internal parameters of the camera have been presented. These techniques are simple (only linear equations need to be solved) and quite robust to noise. The techniques do not require any calibration patterns, unlike most existing techniques. Also, no point-to-point matching is required; image scenes with stable edges are sufficient. No initial estimate of focal length is required. The technique solves for the internal parameters independent of the external parameters. Using this technique an active camera can automatically calibrate itself.

Chapter 4

Robot Calibration

This chapter presents a technique for the *kinematic calibration* of robot manipulators. It is shown that a robot manipulator, with a vision system mounted on it, can calibrate itself by performing a series of motions.

4.1 Introduction

The purpose of a robot kinematic calibration algorithm is to improve the actual kinematic parameters of the robot model which describe the position and orientation of the end-effector relative to the robot base. Most of the kinematic calibration techniques [David et al. 1991, Renders et al. 1991, Vietschegger and Wu 1988], discussed in chapter 2 obtain the parameters by performing large scale non-linear optimizations. In these methods the equations involved are complex and the algorithms are computationally intensive.

The *kinematic calibration* technique developed in this thesis is simpler and involves solving linear equations. In this method only one link is calibrated at a time; as a result the dimensionality of the calibration problem is reduced. The D-H kinematic model described in chapter 1, with four link parameters (l_i, α_i, d_i, θ_i) is used in

the calibration method, since it is adequate to represent the robot kinematics and is the most widely used model in industry. In the case of parallel joints an additional parameter (β_i) is introduced, as discussed in section 1.2.1.

In order to calibrate a robot for its kinematic parameters, it is essential to obtain an estimate of the motion of the end-effector as a result of different joint positions. The approach discussed in this thesis uses a vision system to aid the calibration of a robot manipulator. It uses a single camera mounted rigidly onto the robot gripper. This set-up is commonly known as the *eye-in-hand* configuration and is used in various industrial applications where visual feedback is required by the robot to perform its task-such as grasping an object, navigation or automated assembly, etc. In such applications, it is necessary for the robot controller to know the relation between the robot base and end-effector (*robot kinematic calibration*), between the end-effector and the camera (*hand-to-eye calibration*) and between the camera and the world frame (*camera extrinsic calibration*) in order for the robot to efficiently complete its task.

The *eye-in-hand* setup is used to calibrate the kinematic parameters of the robot manipulator. The view of the camera is fixed on a calibration object with known 3D points. The calibration object has a series of squares on a plane surface; the corner points of these squares can be treated as calibration points. The locations of these points relative to a reference frame on the object are obtained. The camera is pre-calibrated for its internal parameters using the active camera calibration techniques presented in chapter 3. The robot manipulator is moved to different positions by moving one joint at a time. The measurements taken are the position and orientation of the camera relative to the object coordinate frame — obtained by performing the camera extrinsic calibration. The values to be computed are the kinematic link parameters. Figure 4.9 shows the basic setup. Some of the notations and terminology used throughout this chapter are listed below.

- G_i: Robot gripper (end-effector) coordinate frame at position i. This is fixed to the robot gripper and moves with the gripper.

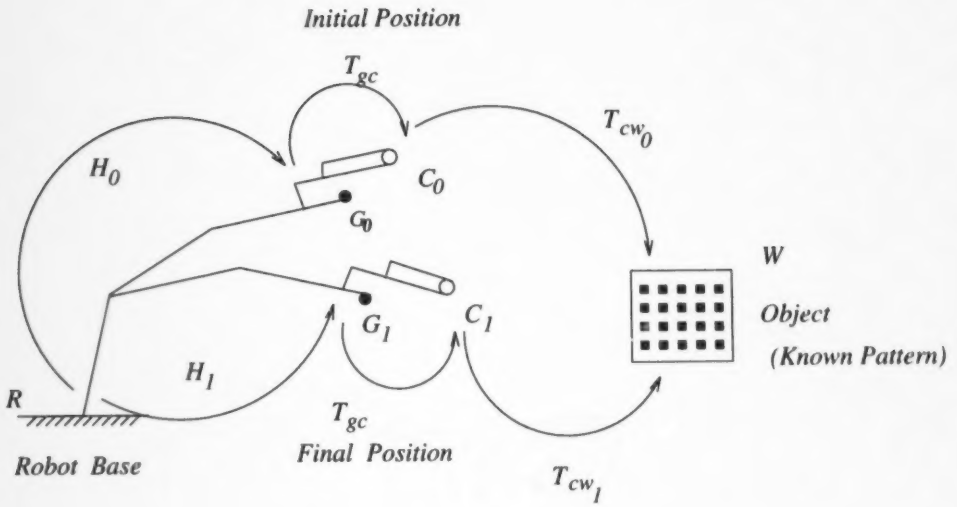

Figure 4.9: Eye-in-Hand System.

- C_i: Camera coordinate system. This is the 3D frame of the camera, with the Z axis along the optical axis, and X and Y axis parallel to the image plane. Since the camera is mounted on the gripper, it moves along with the gripper.
- W: Object coordinate frame, which is fixed on the object and the 3D positions of points on the object are known relative to this frame.
- R: Robot base frame, which is fixed on the base of the robot.
- H_i: Transformation from robot base frame to gripper frame at position i.
- T_{gc}: The transformation from G_i to C_i. This is constant throughout for all motions of the robot as the camera is mounted rigidly on the gripper.
- T_{cw_i}: The transformation from C_i to W.
- T_{rw_i}: The transformation from coordinate frame of joint i to W.
- A_{n_i}: The transformation for link n at position i.
- $(X_{w_i}, Y_{w_i}, Z_{w_i})$: 3D point on the calibration object.
- (x_i, y_i): 2D point in the image.
- c: cos().

- s: sin().

Since camera extrinsic calibration is used in the kinematic calibration procedure, it is discussed first, followed by the robot kinematic calibration technique.

4.2 Camera Extrinsic Calibration

Camera extrinsic calibration involves obtaining the transformation T_{cw} (which consists of a rotation matrix R and a translation vector T) between the camera coordinate frame C and a known reference frame W, which is an arbitrary frame fixed on the calibration object being viewed by the camera. Since the calibration points are on a common surface, the object coordinate frame can be selected such that $Z_{w_i} = 0$. The calibration object has a set of points whose 3D locations are known relative to the reference frame. The camera is calibrated for its external parameters (position and orientation) by relating the 3D reference points and their 2D image locations. In this section, the equations necessary for determining the camera location relative to the object frame are developed. The algorithm for camera extrinsic calibration is presented next. This calibration technique is a modification of the technique developed in [Tsai 1987].

4.2.1 Mathematical Derivations

From camera perspective projection, the image points (x_i, y_i) are related to the known object points $(X_{w_i}, Y_{w_i}, Z_{w_i})$ as follows:

$$x_i = \frac{f_x(r_{11}X_{w_i} + r_{12}Y_{w_i}r_{13}Z_{w_i} + T_x)}{r_{31}X_{w_i} + r_{32}Y_{w_i} + r_{33}Z_{w_i} + T_z}$$

$$y_i = \frac{f_y(r_{21}X_{w_i} + r_{22}Y_{w_i}r_{23}Z_{w_i} + T_y)}{r_{31}X_{w_i} + r_{32}Y_{w_i} + r_{33}Z_{w_i} + T_z}$$

where r_{11}, r_{12},...,r_{31} are the elements of the rotation matrix R; T_x, T_y and T_z are translational elements of T along the x, y and z axes; and f_x and f_y are the focal lengths which are pre-calibrated. Since the object frame is chosen such that $Z_{w_i} = 0$, the above equations would reduce to

$$x_i = \frac{f_x(r_{11}X_{w_i} + r_{12}Y_{w_i} + T_x)}{r_{31}X_{w_i} + r_{32}Y_{w_i} + T_z} \tag{4.1}$$

$$y_i = \frac{f_y(r_{21}X_{w_i} + r_{22}Y_{w_i} + T_y)}{r_{31}X_{w_i} + r_{32}Y_{w_i} + T_z} \tag{4.2}$$

Equating the denominators of the above two equations and simplifying, the following linear equation is obtained with $T_y^{-1}r_{11}$, $T_y^{-1}r_{12}$, $T_y^{-1}r_{21}$, $T_y^{-1}r_{22}$, $T_y^{-1}T_x$ as unknowns:

$$\begin{bmatrix} f_xX_{w_i}y_i & f_xY_{w_i}y_i & f_xy_i & -f_yX_{w_i}x_i & -f_yY_{w_i}x_i \end{bmatrix} \begin{bmatrix} T_y^{-1}r_{11} \\ T_y^{-1}r_{12} \\ T_y^{-1}T_x \\ T_y^{-1}r_{21} \\ T_y^{-1}r_{22} \end{bmatrix} = f_yx_i$$

where $i = 0, 1, \ldots, N-1$. If N, the number of calibration points, is larger than five (the number of unknowns), an overdetermined system of linear equations is obtained which can be solved by a least-squares approach. The value of $|T_y|$ can be obtained from the above five values as follows: define C as a 2×2 matrix such that,

$$C = \begin{bmatrix} r_1 & r_2 \\ r_3 & r_4 \end{bmatrix} = \begin{bmatrix} r_{11}/T_y & r_{12}/T_y \\ r_{21}/T_y & r_{22}/T_y \end{bmatrix}$$

Then, T_y^2 can be computed as (proofs can be found in [Tsai 1987]),

$$T_y^2 = \frac{S - [S^2 - 4(r_1r_4 - r_3r_2)^2]^{1/2}}{2(r_1r_4 - r_3r_2)^2} \tag{4.3}$$

where, $S = r_1^2 + r_2^2 + r_3^2 + r_4^2$. The value of $| T_y |$ is:

$$| T_y | = \sqrt{\frac{S - [S^2 - 4(r_1r_4 - r_3r_2)^2]^{1/2}}{2(r_1r_4 - r_3r_2)^2}} \tag{4.4}$$

To obtain the sign of T_y the following procedure is used,

1. An object point (X_{w_i}, Y_{w_i}, Z_{w_i}), whose image coordinates (x_i, y_i), are away from the image center, is picked.
2. The sign of T_y is assumed to be positive.
3. The following values are computed,

$$r_{11} = (T_y^{-1})r_{11}(T_y) \tag{4.5}$$

$$r_{12} = (T_y^{-1})r_{12}(T_y) \tag{4.6}$$

$$r_{21} = (T_y^{-1})r_{21}(T_y) \tag{4.7}$$

$$r_{22} = (T_y^{-1})r_{22}(T_y) \tag{4.8}$$

$$T_x = (T_y^{-1})T_x(T_y) \tag{4.9}$$

$$x_c = r_{11}X_w + r_{12}Y_w + T_x$$

$$y_c = r_{21}X_w + r_{22}Y_w + T_y$$

4. If (x_c and x_i) and (y_c and y_i) have the same sign, then the sign of T_y is positive, else sign of T_y is negative. This is because, from equations (1.1) and (1.2), both f and z are positive. Hence, the sign of x_i and x_c are the same.

Once the sign of T_y has been determined, the values of r_{11}, r_{12}, r_{21} and r_{22} can be determined from equations (4.4) to (4.8). A rotation matrix (R) can be described as a series of rotations around the x, y, and z axes.

$$R = Rot(z,\phi)Rot(y,\theta)Rot(x,\psi)$$

$$R = \begin{bmatrix} \mathrm{c}\phi\mathrm{c}\theta & \mathrm{c}\phi\mathrm{s}\theta\mathrm{s}\psi - \mathrm{s}\phi\mathrm{c}\psi & \mathrm{c}\phi\mathrm{s}\theta\mathrm{c}\psi + \mathrm{s}\phi\mathrm{s}\psi \\ \mathrm{s}\phi\mathrm{c}\theta & \mathrm{s}\phi\mathrm{s}\theta\mathrm{s}\psi + \mathrm{c}\phi\mathrm{c}\psi & \mathrm{s}\phi\mathrm{s}\theta\mathrm{c}\psi - \mathrm{c}\phi\mathrm{s}\psi \\ -\mathrm{s}\theta & \mathrm{c}\theta\mathrm{s}\psi & \mathrm{c}\theta\mathrm{c}\psi \end{bmatrix} = \begin{bmatrix} r_{11} & r_{12} & r_{13} \\ r_{21} & r_{22} & r_{23} \\ r_{31} & r_{32} & r_{33} \end{bmatrix} \tag{4.10}$$

Since r_{11}, r_{12}, r_{21} and r_{22} are known, equating the terms on the L.H.S would give values for θ, ψ and ϕ. But the value of θ is not unique, as the value of $\cos\theta$ is obtained, and the sign of θ could be either positive or negative. In order to obtain the correct values for the rotation matrix, the following procedure is used:

1. Assume the sign of θ to be positive. Compute the rotation matrix according to equation (4.9).
2. Using this rotation matrix, compute the values of f_x (f_y) and T_z by solving the linear equation (4.1).
3. If the sign of f_x is negative, then the rotation matrix is wrong; change the sign of θ to negative. Compute the right rotation matrix.

Once the rotation matrix has been computed, the value of T_z can be computed as follows, from equations (4.1) and (4.2) by using a least squares solution.

$$T_z = \frac{f_x}{x_i}(r_{11}X_{w_i} + r_{12}Y_{w_i} + T_x) - (r_{31}X_{w_i} + r_{32}Y_{w_i})$$
$$T_z = \frac{f_y}{y_i}(r_{21}X_{w_i} + r_{22}Y_{w_i} + T_y) - (r_{31}X_{w_i} + r_{32}Y_{w_i})$$

4.2.2 Camera Extrinsic Calibration Algorithm

The camera extrinsic calibration procedure can be outlined as follows:

- Grab an image of the calibration object. Obtain the (x_i, y_i) image coordinates for corresponding object points $(X_{w_i}, Y_{w_i}, Z_{w_i})$.
- Compute the rotational parameters and translational elements, T_x and T_y of the transformation matrix, T_{cw} using equations (4.8) to (4.9).
- Using the above values, compute the value of T_z using equations (4.1) and (4.2).

The extrinsic parameters computed by this algorithm are used to compute the kinematic model parameters of the robot manipulator.

4.3 Robot Calibration

In this section, an incremental calibration procedure to determine the parameters of the kinematic model of a robot manipulator is developed. The setup used for the kinematic calibration is as follows: a camera is mounted rigidly on the end-effector and the view fixed on a calibration object with known 3D points. In order to reduce the complexity of the calibration problem, one link is calibrated at a time. As the D-H model is used, only four parameters are to be estimated at a time (in the case of parallel joints, the number of parameters is five). For an $n-$link manipulator the last (n^{th}) link is calibrated first, then the $(n-1)^{th}$ link and so on. The robot manipulator carrying the camera makes a series of moves, by moving the joints to different positions, and at the end of each move an image of the object is grabbed by the camera. Figure 4.9 shows the *transform graph* for the eye-in-hand system. The *transform equations* for the two positions ($i = 0$ and $i = 1$) of the robot obtained as a result of end-effector motion are,

$$\left.\begin{aligned} R &= H_0 T_{gc} T_{cw_0} \\ R &= H_1 T_{gc} T_{cw_1} \end{aligned}\right\} \Rightarrow H_0 T_{gc} T_{cw_0} = H_1 T_{gc} T_{cw_1} \tag{4.11}$$

where H_0 is the transformation for position $i = 0$ and H_1 for $i = 1$.

In the above equation, the value of T_{cw_i} can be obtained by performing the *camera extrinsic calibration* discussed in section 4.2, for which an image of the calibration object at position i is captured. The transformation T_{gc} is known and is constant at any position as the camera is mounted rigidly on the end-effector. Methods to calculate T_{gc} are found in [Shiu and Ahmad 1989, Tsai and Lenz 1989]. The transformation H_i consists of the link parameters, which have to be determined. Some propositions are presented to support the kinematic calibration of the robot manipulator. An algorithm is developed next. Though this method is generic and applicable to an n-link robot, a two-link robot manipulator is considered and equations are developed. The algorithm is then generalized for a n-link robot manipulator.

4.3.1 Mathematical Derivations

The equations for solving the kinematic parameters of the robot model are developed for a two-link robot manipulator (link 2, the distal joint and link 1 as shown in figure 4.10) with revolute joints. First, link 2 parameters are calibrated followed by link 1 parameters. It is assumed that an estimate of T_{gc} is known. Using the D-H model, the link parameters to be estimated are l_i, α_i, d_i and $\delta\theta_i$ (the error in the encoder reading). An estimate of the joint angle (θ_i) is given by the encoders mounted on the robot manipulator.

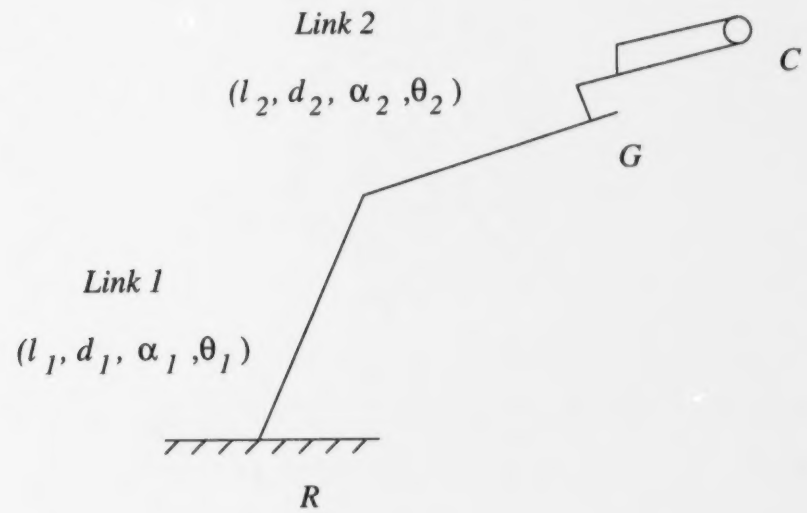

Figure 4.10: A Two-link Manipulator with D-H Model Parameters.

Proposition 4.1 *Linear equations in the kinematic parameters l_2, α_2 and $\delta\theta_2$ of link 2 can be obtained by moving only joint 2, (thereby moving the end-effector to a different position), keeping joint 1 at a fixed position.*

The transform equation obtained by moving only joint 1 from position 0 (θ_{2_0}) to position 1 (θ_{2_1}) (shown in figure 4.11), is

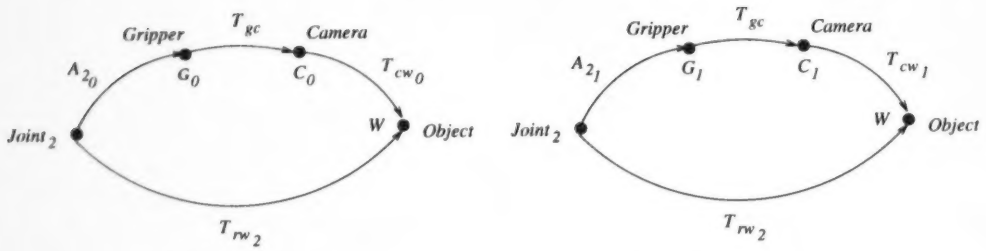

(a) Initial Position (i = 0).

(b) Final Position (i = 1).

Figure 4.11: Transform Graphs for Movement of Joint 2.

$$\left.\begin{aligned} T_{rw_2} &= A_{2_0} T_{gc} T_{cw_0} \\ T_{rw_2} &= A_{2_1} T_{gc} T_{cw_1} \end{aligned}\right\} \Rightarrow A_{2_1}^{-1} A_{2_0} = T_{gc} T_{cw_1} T_{cw_0}^{-1} T_{gc}^{-1} \tag{4.12}$$

Let the R.H.S of the equation, which is known, be represented by the matrix

$$R = \begin{bmatrix} r_{11} & r_{12} & r_{13} \\ r_{21} & r_{22} & r_{23} \\ r_{31} & r_{32} & r_{33} \end{bmatrix}$$

The link parameters can be obtained by solving a set of linear equations as follows. The link transformation (A_i) of the D-H model is given by

$$A_i = Rot(z, \theta_i) Trans(0, 0, d_i) Trans(l_i, 0, 0) Rot(x, \alpha_i)$$

$$A_i = \begin{bmatrix} \mathsf{c}\theta_i & -\mathsf{s}\theta_i \mathsf{c}\alpha_i & \mathsf{s}\theta_i \mathsf{s}\alpha_i & l_i \mathsf{c}\theta_i \\ \mathsf{s}\theta_i & \mathsf{c}\theta_i \mathsf{c}\alpha_i & -\mathsf{c}\theta_i \mathsf{s}\alpha_i & l_i \mathsf{s}\theta_i \\ 0 & \mathsf{s}\alpha_i & \mathsf{c}\alpha_i & d \\ 0 & 0 & 0 & 1 \end{bmatrix} \tag{4.13}$$

and,

$$A_i^{-1} = Rot(x, \alpha_i)^{-1} Trans(l_i, 0, 0)^{-1} Trans(0, 0, d_i)^{-1} Rot(z, \theta_i)^{-1}$$

$$A_i^{-1} = \begin{bmatrix} c\theta_i & s\theta_i & 0 & -l_i \\ -s\theta_i c\alpha_i & c\theta_i c\alpha_i & s\alpha_i & -d_i s\alpha_i \\ s\theta_i s\alpha_i & -c\theta_i s\alpha_i & c\alpha_i & -d_i c\alpha_i \\ 0 & 0 & 0 & 1 \end{bmatrix} \tag{4.14}$$

Simplifying and equating the terms on the L.H.S of the equation (4.12) (which contains the link parameters) to the elements of R (which are known), the following set of linear equations can be obtained,

$$c\theta_{2_1} c\theta_{2_0} + s\theta_{2_1} s\theta_{2_0} = r_{11} \tag{4.15}$$

$$c\alpha_2(-s\theta_{2_1} c\theta_{2_0} + c\theta_{2_1} s\theta_{2_0}) = r_{21} \tag{4.16}$$

$$s\alpha_2(-c\theta_{2_1} s\theta_{2_0} + s\theta_{2_1} c\theta_{2_0}) = r_{31} \tag{4.17}$$

$$c\alpha_2(-c\theta_{2_1} s\theta_{2_0} + s\theta_{2_1} c\theta_{2_0}) = r_{12} \tag{4.18}$$

$$c^2\alpha_2(s\theta_{2_1} s\theta_{2_0} + c\theta_{2_1} c\theta_{2_0}) + s^2\alpha_2 = r_{22} \tag{4.19}$$

$$c\alpha_2 s\alpha_2(-s\theta_{2_1} s\theta_{2_0} - c\theta_{2_1} c\theta_{2_0} + 1) = r_{23} \tag{4.20}$$

$$s\alpha_2(-s\theta_{2_1} c\theta_{2_0} + c\theta_{2_1} s\theta_{2_0}) = r_{13} \tag{4.21}$$

$$c\alpha_2 s\alpha_2(-s\theta_{2_1} s\theta_{2_0} - c\theta_{2_1} c\theta_{2_0} + 1) = r_{32} \tag{4.22}$$

$$s^2\alpha_2(s\theta_{2_1} s\theta_{2_0} + c\theta_{2_1} c\theta_{2_0}) + c^2\alpha_2 = r_{33} \tag{4.23}$$

$$l_2(c\theta_{2_1} c\theta_{2_0} + s\theta_{2_1} s\theta_{2_0} - 1) = r_{14} \tag{4.24}$$

$$l_2(-s\theta_{2_1} c\theta_{2_0} c\alpha_2 + c\theta_{2_1} s\theta_{2_0} c\alpha_2) = r_{24} \tag{4.25}$$

$$l_2(s\theta_{2_1} c\theta_{2_0} s\alpha_2 - c\theta_{2_1} s\theta_{2_0} s\alpha_2) = r_{34} \tag{4.26}$$

An estimate of l_2 is obtained from equations (4.15) and (4.24) as,

$$l_2 = \frac{r_{14}}{r_{11} - 1} \tag{4.27}$$

An estimate of $\tan\alpha_2$ can be obtained by dividing equation (4.21) by equation (4.16), from which α_2 can be obtained.

$$\frac{s\alpha_2}{c\alpha_2} = \frac{r_{13}}{r_{21}} \Rightarrow \alpha_2 = \tan^{-1}\frac{r_{13}}{r_{21}} \tag{4.28}$$

In order to obtain the joint offset readings, consider equation (4.15). If θ_{2_0} is 0 deg (i.e. the first position of the link is its zero position), the value of θ_{2_1} is given by

$$\mathsf{c}\theta_{2_1} = r_{11} \Rightarrow \theta_{2_1} = \mathsf{c}^{-1} r_{11} \tag{4.29}$$

This difference between this value of θ_{2_1} and the encoder reading would give the offset value $\delta\theta_2$.

The value of d_2 cannot be obtained from this set of equations. The value of d_2 is obtained along with the link parameters of link 1.

Proposition 4.2 *The kinematic parameters of link 1, l_1, α_1, $\delta\theta_1$ and the link 2 parameter d_2 can be obtained by moving the first joint, given the estimates of other three link 2 parameters.*

The transform equation obtained by moving only joint 1, (joint 2 is fixed at its zero position, $\theta_2 = 0$, to simplify the equations), from position 0 (θ_{1_0}) to position 1 (θ_{1_1}), shown in figure 4.12, is

$$\left.\begin{aligned} T_{rw_1} &= A_{1_0} A_{2_0} T_{gc} T_{cw_0} \\ T_{rw_1} &= A_{1_1} A_{2_0} T_{gc} T_{cw_1} \end{aligned}\right\} \Rightarrow A_{1_1}^{-1} A_{1_0} = A_{2_0} T_{gc} T_{cw_1} T_{cw_0}^{-1} T_{gc}^{-1} A_{2_0}^{-1} \tag{4.30}$$

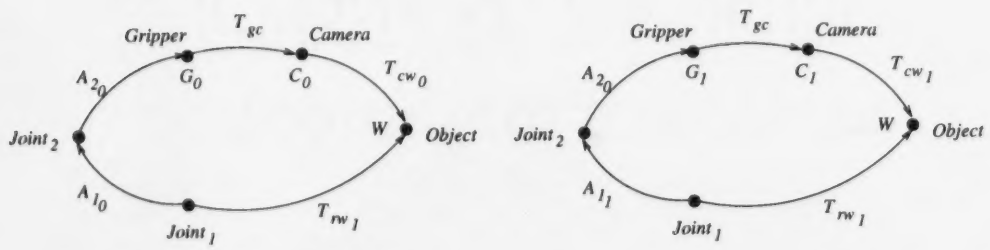

(a) Initial Position (i = 0).

(b) Final Position (i = 1).

Figure 4.12: Transform Graphs for Movement of Joint 1.

The elements of the R.H.S are known, except for d_2. Let the term $T_{gc}T_{cw_1}T_{cw_0}^{-1}T_{gc}^{-1}$ be represented by matrix R as in the proposition (4.1). By equating the terms of L.H.S which contain the link 1 parameters, to the elements of R.H.S and simplifying the following equations are obtained,

$$\frac{\mathsf{s}\alpha_1}{\mathsf{c}\alpha_1} = \frac{r_{31}\mathsf{c}\alpha_2 - r_{21}\mathsf{s}\alpha_2}{r_{21}\mathsf{c}\alpha_2 + r_{31}\mathsf{s}\alpha_2} \Rightarrow \alpha_1 = \tan^{-1}\frac{r_{31}\mathsf{c}\alpha_2 - r_{21}\mathsf{s}\alpha_2}{r_{21}\mathsf{c}\alpha_2 + r_{31}\mathsf{s}\alpha_2} \tag{4.31}$$

The joint offset is given as follows. Let θ_{1_0} be 0 deg (i.e. the first position of link 1 is its zero position), the value of θ_{1_1} is given by.

$$\mathsf{c}\theta_{1_1} = r_{11} \Rightarrow \theta_{1_1} = \mathsf{c}^{-1}r_{11} \tag{4.32}$$

This difference between this value of θ_{1_1} and the encoder reading gives the offset value $\delta\theta_1$.

Two linear equations in l_1 and d_2 are obtained which can be solved to obtain their estimates,

$$l_1(r_{11} - 1.0) + d_2(r_{12}\mathsf{s}\alpha_2 + r_{13}\mathsf{c}\alpha_2) = r_{14} + l_2(1.0 - r_{11}) \tag{4.33}$$

$$l_1(r_{21}) + d_2(r_{22}\mathsf{s}\alpha_2 + r_{23}\mathsf{c}\alpha_2) = r_{24} - l_2(r_{21}) \tag{4.34}$$

These equations can be easily modified for the case, when joint 2 is not at its zero position. The estimates can be improved iteratively by moving the joints to different positions ($i = 0, 1, ..., N$) and estimating the parameter values each time. With the above discussed method, estimate of the link 1 parameter d_1 cannot be obtained. This parameter can be estimated by using an initial estimate and iteratively refining it. Consider the transform equation (shown in figure 11 (a)),

$$T_{rw_1} = A_{1_0}A_{2_0}T_{gc}T_{cw_0} \tag{4.35}$$

A set of equations can be obtained with the elements of T_{rw_1} and d_1 as unknown. These equations can be solved iteratively, by moving the joint 1 to different positions, with an initial estimate of d_1.

4.3.2 Robot Calibration Algorithm

The equations developed thus far can be generalized to a n-link robot. First the n^{th} link is calibrated by moving joint n, with joints 1 to $n-1$ at a fixed position. Then the $n-1^{th}$ is calibrated and so on. Parameter d_1 has to be estimated with a different approach as discussed earlier for the two-link manipulator. The calibration procedure can be outlined as follows,

Loop until desired accuracy is obtained (T_{gc} is known)

- for $i = n$ downto 1
  - Move joint i
  - Perform camera extrinsic calibration
  - using T_{gc}, calibrate i^{th} link for its parameters l, α and $\delta\theta$, and d with the parameters of link $i-1$ according to proposition (4.1) and (4.2).
  - if ($i = 1$)
    obtain estimate of d by equation (4.35).

4.4 Theoretical Error Analysis

In this section a brief theoretical error analysis is presented for the kinematic calibration algorithm of a two-link robot manipulator. Let the term $T_{gc}T_{cw_1}T_{cw_0}^{-1}T_{gc}^{-1}$ in propositions (4.1 - 4.2) be represented by R. The effect of rotational and translational errors in R on the estimation of link parameters is studied.

Remark 4.1 *Any Rotational errors in R will produce a corresponding error in the estimate of* α_i *and* $\delta\theta_i$.

Proof: As can be seen from equations (4.28) and (4.29), the values of α_2 and $\delta\theta_2$ are dependent on the rotational parameters of R. Thus any error in the rotational

parameters would produce a corresponding error in their estimates. Similarly for the link 1 parameters α_1 and $\delta\theta_1$.

Remark 4.2 *Any rotational or translational errors will produce an error in the estimate of* l_i.

Proof: As seen from equation (4.27) the value of l_2 is dependent on both rotational and translational parameters of R. Hence, any errors in these terms would produce an error in l_2. Similarly for l_1.

Remark 4.3 *Errors in estimates of* α_2 *will produce errors in* α_1.

Proof: From equation (4.31) it can be seen that the value of α_1 depends on the estimates of α_2. Hence any error in this term would produce significant error in α_1.

Remark 4.4 *Errors in* α_2 *and* l_2 *will produce errors in* l_1 *and* d_2.

Proof: It can be seen from equations (4.33) and (4.34) that values of l_1 and d_2 are proportional to l_2 and α_2. Hence the errors in these link 2 parameters would cause errors in l_1 and d_2.

4.5 Conclusions

In this chapter a calibration procedure to determine the kinematic parameters of a robot manipulator with the aid of a camera is presented. The technique requires knowledge of hand-to-eye transformation [Shiu and Ahmad 1989, Tsai and Lenz 1989]. This method is simpler as it formulates the problem as a set of linear equations instead of the non-linear solutions proposed elsewhere. Since calibration is performed incrementally one link at a time, the complexity of the algorithm is reduced.

Chapter 5

Experimental results

This chapter presents a few experimental results and observations obtained by implementing the camera and robot calibration techniques presented in chapters 3 and 4.

5.1 Active camera calibration

In this section some of the results obtained by performing the active calibration strategies are presented. Initially, simulation results using synthetic data are provided followed by real experiments with a camera. The results of Strategy A and Strategy B are also provided for completeness [Basu 1993].

5.1.1 Simulations

Simulations were carried out using synthetic data. Sets of 3D points were randomly generated to represent contours. These points were then projected on to the image plane and the values quantized to the nearest integer to represent the image pixels. Tests were performed without noise and with adding Gaussian noise.

First, the performance results of Strategy A and B are presented. Table 5.1

summarizes some of the results obtained without noise. In order to study the variation of error in focal length estimate, the values of f_x and f_y were varied between 100 and 1000 in steps of 100, keeping all the other parameters fixed. The values of pan/tilt angles were fixed at 3 deg. Figure 5.13 shows the results obtained. The effect of discretization error seems to influence the estimates of Strategy A more at smaller focal lengths. This is because Strategy A is not very robust to noise. When the focal length is large, the discretization error is relatively smaller[1]. Thus Strategy A produced better results with larger focal lengths. The errors in the estimates obtained by Strategy B do not change rapidly with increasing focal length. This is because Strategy B is theoretically less accurate than Strategy A as several terms were ignored in deriving the equations.

Strategy	Points Used	f_x	f_y	f_x^e	f_y^e
A	10	400	600	397	604
A	30	400	600	405	605
A	10	600	700	584	707
A	30	600	700	599	703
B	10	400	600	405	607
B	30	400	600	404	593
B	10	600	700	610	692
B	30	600	700	606	696

Table 5.1: Simulation Results of Strategy A and B Without Noise.

Next, Gaussian noise was added to the image points to test the robustness of the strategies to noise. Strategy A performed quite poorly, producing estimates with 20, 28 and 40 percent errors when the noise had a standard deviation (σ) of 3, 4, and 5 respectively — indicating that Strategy A is sensitive to noise. Strategy B produced reliable estimates, (10 percent error), even when σ was as large as 20. Figure 5.14 shows the error in estimating focal length by Strategy B with noise, with focal lengths f_x and f_y as 400 and 600 respectively. Thus Strategy B is more robust to noise, though

[1]The interpixel distance measured in terms of the focal length is $\frac{1}{f_x}$ ($\frac{1}{f_y}$) in the x (y) direction. When focal length is increased the discretization error, relative to the focal length is decreased.

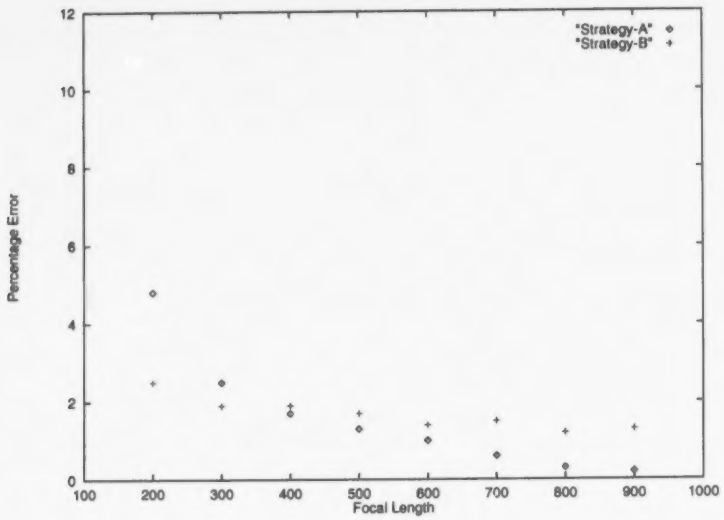

Figure 5.13: Variation of Error in Focal Length.

Strategy A is theoretically more accurate. This can be explained by Propositions (3.3) and (3.5). When the camera pans by a small angle (3-4 degrees), $(\overline{y_p} - \overline{y})$ had values less than 2 pixels, whereas $(\overline{x_p} - \overline{x})$ was as large as 30-40 pixels. Strategy A uses terms such as $(\overline{y_p} - \overline{y})$ which are affected by noise of fewer pixels than $(\overline{x_p} - \overline{x})$, used by Strategy B.

The performances of Strategy C and Strategy D in computing the focal length and image center were studied. Initially, tests were conducted by varying the roll angle in Strategy C. Gaussian noise was added to the image points to study the effect of noise on the error in computing the image center. The focal lengths, f_x and $f_y$were fixed at 400 and 600, and δ_x and δ_y at 10 and 20 pixels respectively. Table 5.2 summarizes the results obtained in computing the image center. Figure 5.15 shows the variation of error in computed the image center with roll angle when Gaussian noise with standard deviation (σ) of 0 (no noise), 5, 10 and 15 pixels was added. It can be seen that the error decreases as roll angle increases. This is because the change in image coordinates is greater at larger roll angles, resulting in a smaller relative error. Also, Strategy C performs reasonably well in determining the image center even when σ is as large as 15.

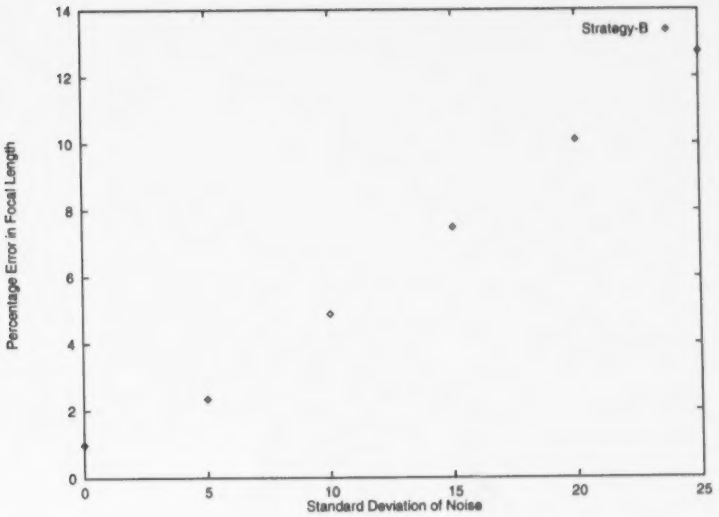

Figure 5.14: Variation of Error in Focal Length with Noise (Strategy B).

Angle (deg)	Points Used	δ_x	δ_y	$\sigma = 0$		$\sigma = 5$		$\sigma = 10$	
				δ_x^e	δ_y^e	δ_x^e	δ_y^e	δ_x^e	δ_y^e
20	50	10	20	11	22	12	23	12	23
40	50	10	20	11	21	12	22	12	19
60	50	10	20	11	21	12	21	13	21
80	50	10	20	11	21	11	21	11	22
100	50	10	20	10	21	10	21	11	21
120	50	10	20	11	21	11	21	11	21
140	50	10	20	11	21	11	21	11	21
160	50	10	20	10	21	11	21	11	21
180	50	10	20	10	20	10	21	10	21

Table 5.2: Simulation Results of Strategy C in Computing Image Center

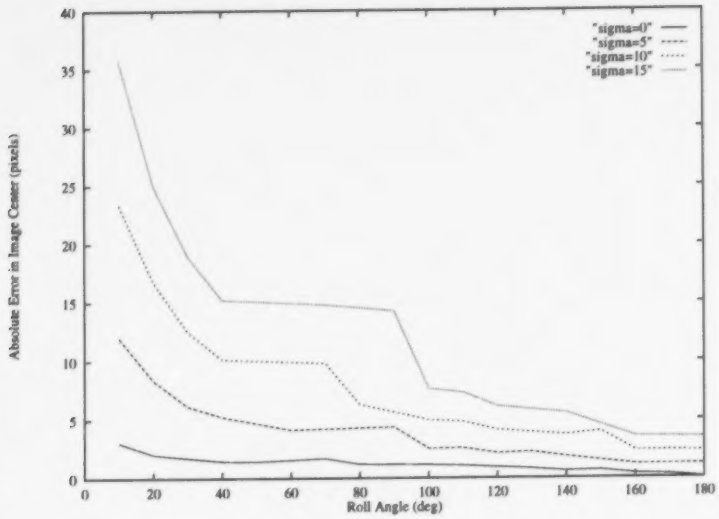

Figure 5.15: Variation of Error in Image Center with Roll Angle and Noise.

Table 5.3 summarizes the results obtained by Strategy D. The results for image center obtained by Strategy D are almost similar to the ones produced by Strategy C when roll angle is 180 deg, as seen in Figure 5.16. This is because with roll angle equal to 180 deg the equations used by Strategy C reduce to those in Strategy D. Strategy D, however, is a little more accurate as the equations are obtained directly without using the estimates of f_x and f_y. Table 5.4 summarizes the results of focal length estimates obtained by Strategy C and Strategy D. The focal lengths obtained by Strategy D are similar to those produced by Strategy C, although Strategy D is theoretically more accurate, which can be seen from Figure 5.17. This justifies ignoring small terms in computing the focal length by Strategy C (which essentially uses Strategy B). But as the noise is increased Strategy D produces more reliable results than Strategy C (as the relative error increases).

Points Used	δ_x	δ_y	$\sigma = 0$		$\sigma = 5$		$\sigma = 10$	
			δ_x^e	δ_y^e	δ_x^e	δ_y^e	δ_x^e	δ_y^e
50	10	20	10	20	11	20	11	20

Table 5.3: Simulation Results of Strategy D in Computing Image Center

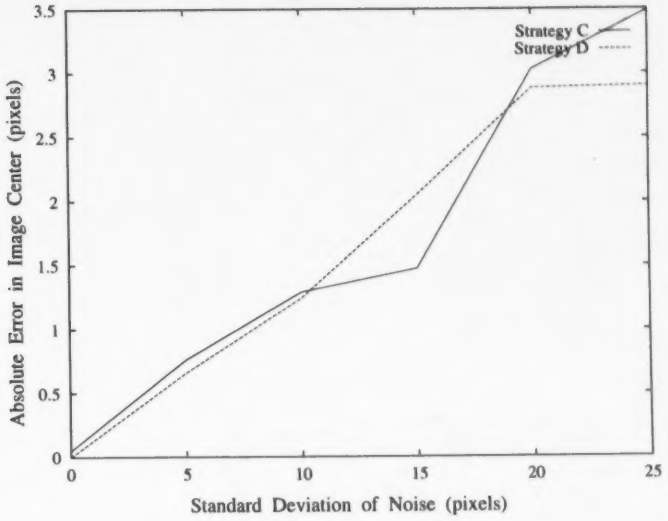

Figure 5.16: Comparison of Strategy C and Strategy D in Computing Image Center.

Strategy	Points Used	f_x	f_y	$\sigma = 0$		$\sigma = 5$	
				f_x^e	f_y^e	f_x^e	f_y^e
C	50	400	600	403	602	396	603
D	50	400	600	401	601	403	599

Table 5.4: Simulation Results in Estimating Focal Length

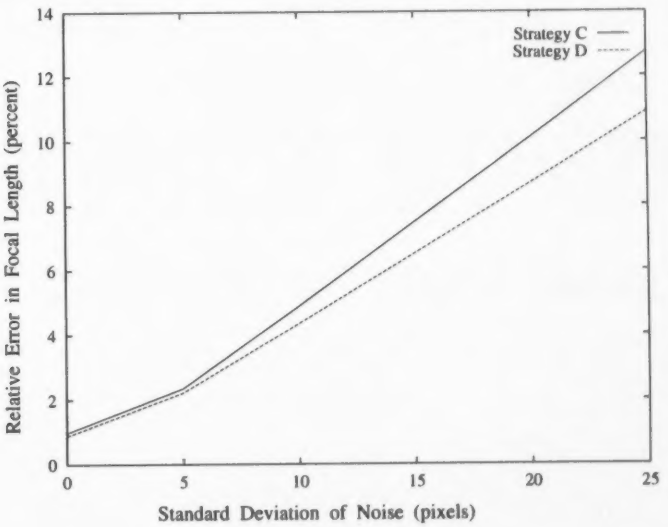

Figure 5.17: Comparison of Strategy C and Strategy D in Computing Focal Length.

Next, tests were performed by introducing an error in the axis of rotation. These showed that when the axis is parallel to the camera axis, the errors in δ_x and δ_y are insignificant if the depth is large compared to the deviation of the axis from the camera center (as seen from Figure 5.18). Then, tests were performed by introducing errors of 1, 2 and 3 degrees in the axis of rotation, and roll angle equal to 180 deg. Figure 5.19 and 5.20 show the error in δ_x and δ_y when the axis of rotation lies in the yz plane and the xz plane. It can be seen that the error in δ_x is insignificant, whereas the error in δ_y is increasing proportionately with the error angle when the axis lies in the xz plane. Similarly, the error in δ_x is large when the axis lies in the xz plane. Thus any error in the axis of rotation results in a considerable amount of error in computing the image center.

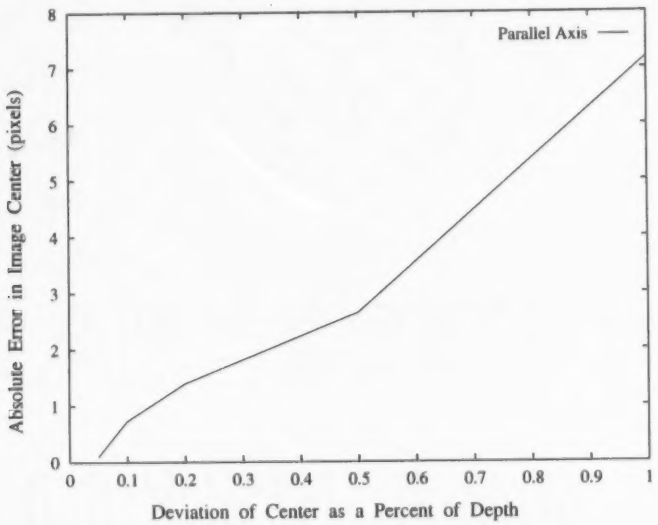

Figure 5.18: Error in δx and δy when Axis of Rotation is Parallel to the Camera z axis.

5.1.2 Experiments with Real Images

The active calibration algorithms were tested on a real system. The active platform in our laboratory with the COHU camera was used to acquire images. Strategies A and B were used to obtain the focal lengths. In order to perform the active calibration

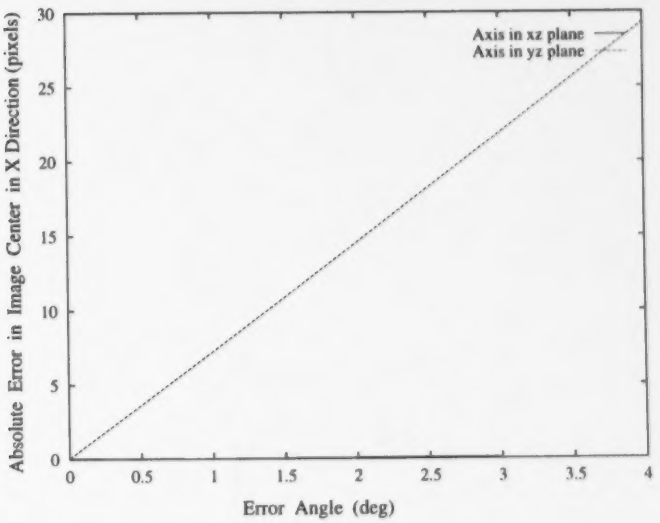

Figure 5.19: Error in δx with Error in Axis of Rotation (at an angle to the camera z axis).

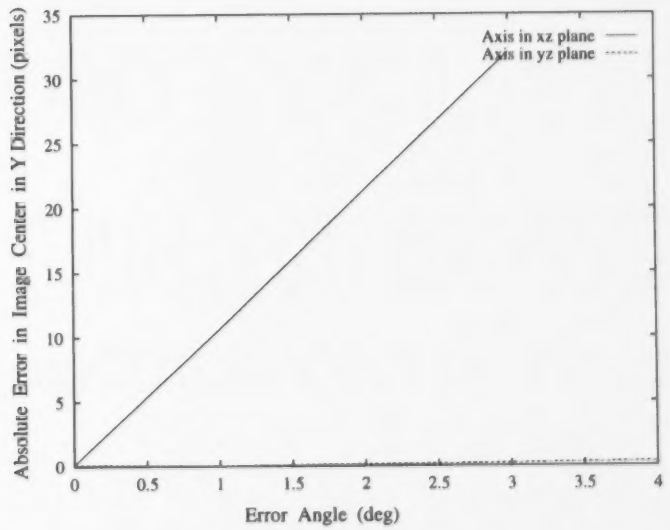

Figure 5.20: Error in δy with Error in Axis of Rotation (at an angle to the camera z axis).

procedures automatically, it is necessary to match contours of interest during pan/tilt motions of the camera. This was done by tracking image contours over the initial and pan/tilt images. First, edges in the images were obtained. Edges in the original image, within a specific window, were thickened using the morphological operation of "dilation" [Maragos 1987]. Then, edges in the pan/tilt images were AND-ed with the dilated original image to obtain the corresponding image contours. The observation that contours move horizontally (vertically) during a pan (tilt) motion of the camera was taken into account to design the matching algorithm. Figure 5.21 shows a sequence of original and panned images. The corresponding edges with the tracked contours within the specified window are illustrated in Figure 5.22. Figures 5.23 and 5.24 show a sequence of initial and tilted images and the corresponding edges.

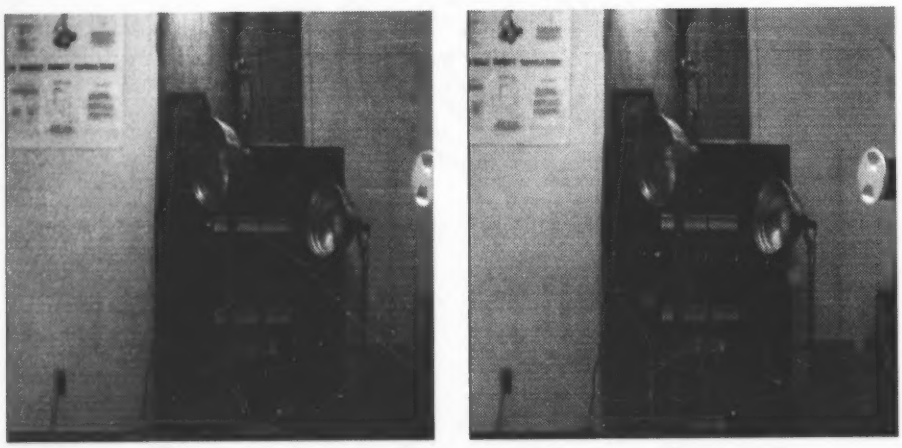

(a) Initial Image. (b) Image after Pan.

Figure 5.21: Image Sequence.

Using Strategy A, the estimates of f_x and f_y were 700 and 985, while Strategy B produced estimates of 910 and 1120 respectively. The values were also obtained by using a calibration procedure similar to one in [Slama 1980] which uses a known pattern (known 3D points). Starting with an initial estimate, the values were refined using a least squares approach to minimize the error between observed and predicted

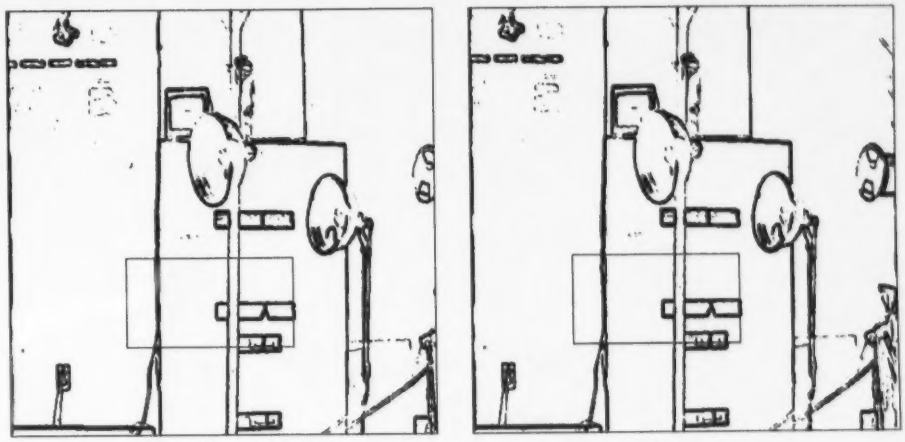

(a) Edges of Initial Image.

(b) Edges after Pan.

Figure 5.22: Edges of Image Sequence.

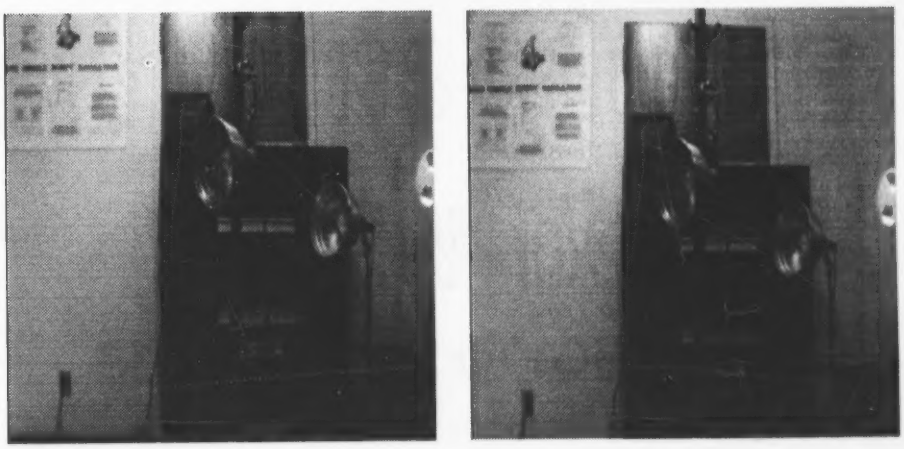

(a) Initial Image.

(b) Image after Tilt.

Figure 5.23: Image Sequence.

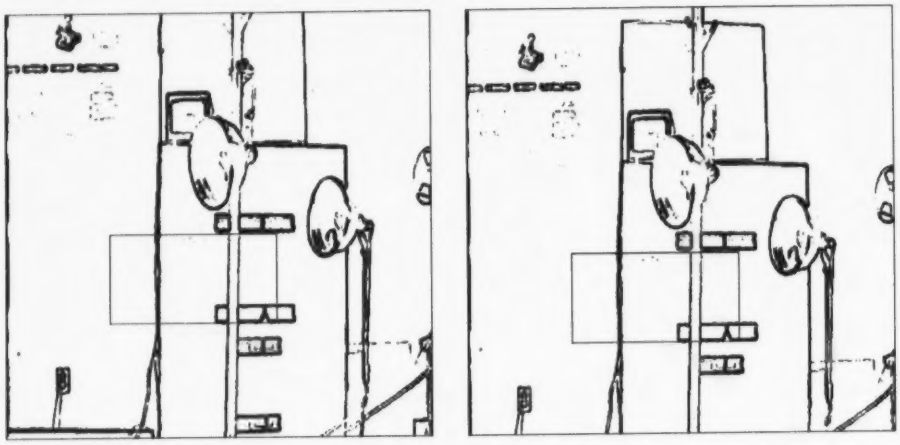

(a) Edges of Initial Image. (b) Edges after Tilt.

Figure 5.24: Edges of Image Sequence.

locations of the points. The values of f_x and f_y obtained by this procedure were 890 and 1109. The values estimated by Strategy B were more stable than those obtained by Strategy A. The value of $(\overline{y} - \overline{y_t})$ and $(\overline{x} - \overline{x_p})$ were in the range of 30-40 pixels, whereas $(\overline{x} - \overline{x_t})$ and $(\overline{y} - \overline{y_p})$ were around 1-2 pixels. The pan/tilt angles, which were obtained from measurements from the potentiometer mounted on the camera, were around 3 degrees. The errors in computed focal lengths are partly due to errors in measured angles. Image center estimates obtained by Strategy A and Strategy B were unstable as terms such as $(\overline{x} - \overline{x_t})$, which are sensitive to noise, are used in estimating the values.

Strategies C and D were used to compute the image center. Roll movements of 90 and 180 degrees only were used. Images of three different scenes were acquired. For each scene, a sequence of three images (initial image, images after roll movements of 90 and 180 degrees) were taken. In order to obtain the corresponding contours in the images, two steps were followed. First, edges were extracted for the images. Edges within a central window in the initial image were tracked over the sequence of images.

Figure 5.25 shows a sequence of images and Figure 5.26 shows the corresponding edges of the image sequence with the tracked (matching) contours within a specified bounding box. Matching of contours was done manually by placing the window over the corresponding edges in the images. Using Strategy C (roll angle of 90 degrees) the estimates of δ_x and δ_y were 2 and 28 respectively. These values were obtained by performing the calculations over different contours and computing the average. Using Strategy D (roll angle of 180 deg) the estimates for δ_x and δ_y were 2 and 30 pixels. The values of δ_x and δ_y, obtained by a technique which uses a predefined pattern, were 4 and 34 pixels. Thus it can be seen that the active calibration algorithms have performed reasonably in real situations, and in addition, the error is smaller when the roll angle is 180 deg rather than 90 degrees.

Figures 5.27 and 5.28 show the images and corresponding edges for the second scene. The estimates for δ_x and δ_y obtained by Strategy C (90 deg roll) were 3 and 29 pixels, while the values obtained by Strategy D were 2 and 30 pixels. Thus it can be seen that the active calibration algorithms produce stable results in real situations. Images for the third scene have not been shown here. The results obtained were similar to the values mentioned for the above two scenes (scene 1 and scene 2). The focal lengths used were initially obtained by the active calibration procedure discussed in Strategy B.

5.2 Robot kinematic calibration

In this section, some of the results obtained by performing the robot calibration procedure developed in Chapter 4 are presented.

(a) Initial Image.

(b) Image after 90 deg Rotation.

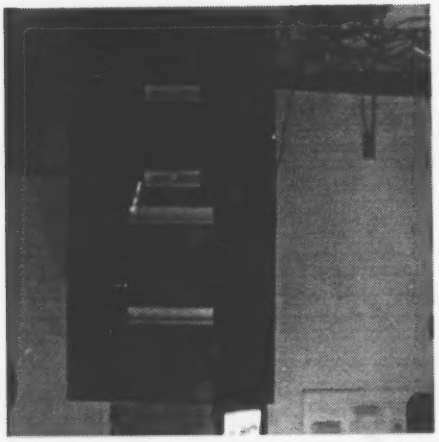

(c) Image after 180 deg Rotation.

Figure 5.25: Sequence of Images Taken (first scene).

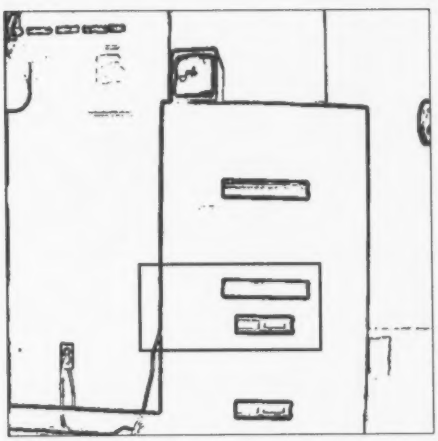

(a) Initial Image.

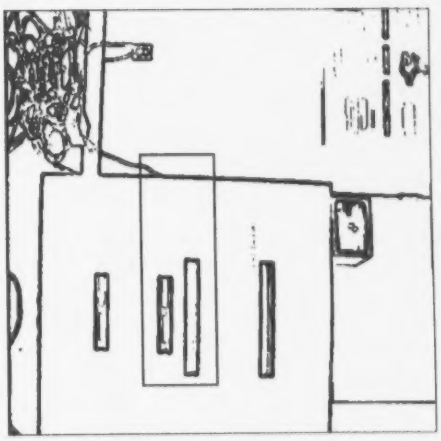

(b) Image after 90 deg Rotation.

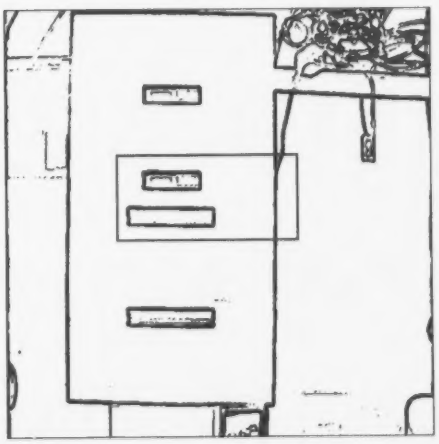

(c) Image after 180 deg Rotation.

Figure 5.26: Corresponding Edges of the Images (first scene).

(a) Initial Image.

(b) Image after 90 deg Rotation.

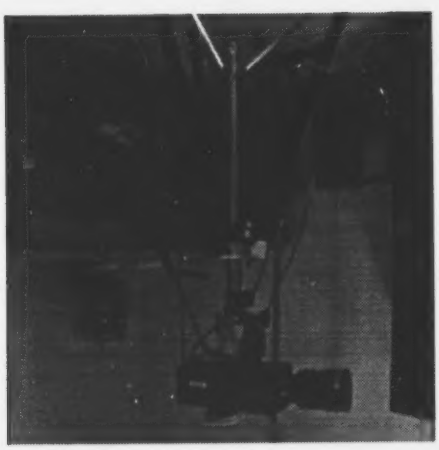

(c) Image after 180 deg Rotation.

Figure 5.27: Sequence of Images Taken (second scene).

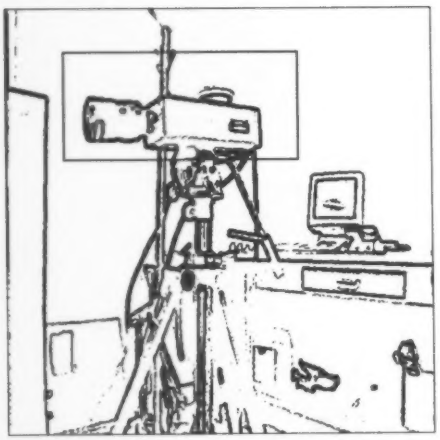

(a) Initial Image.

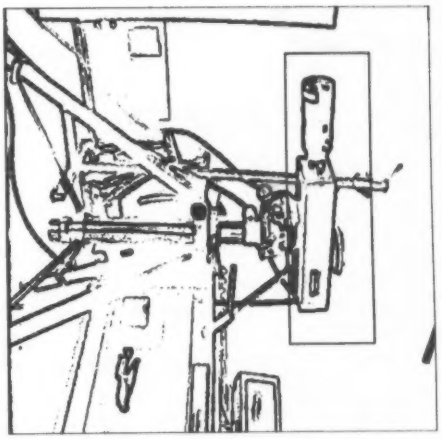

(b) Image after 90 deg Rotation.

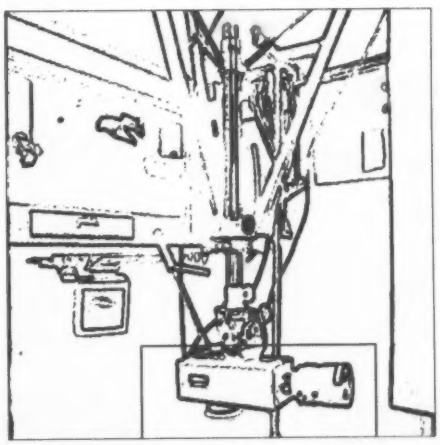

(c) Image after 180 deg Rotation.

Figure 5.28: Corresponding Edges of the Images (second scene).

5.2.1 Simulations

Simulations were carried out using synthetic data. The calibration procedure was used to determine the link parameters of a three link robot with revolute joints (link 1, link 2 and link 3). The robot link parameters were obtained from three links of a PUMA 560 robot arm. A three link robot can be viewed as shown in Figure 5.29. Thus the kinematic parameters to be determined are: link 1 — l_1, α_1, d_1 and $\delta\theta_1$, link 2 — l_2, α_2, d_2 and $\delta\theta_2$, link 3 — l_3, α_3, d_3 and $\delta\theta_3$. Table 5.5 gives the actual values for these parameters.

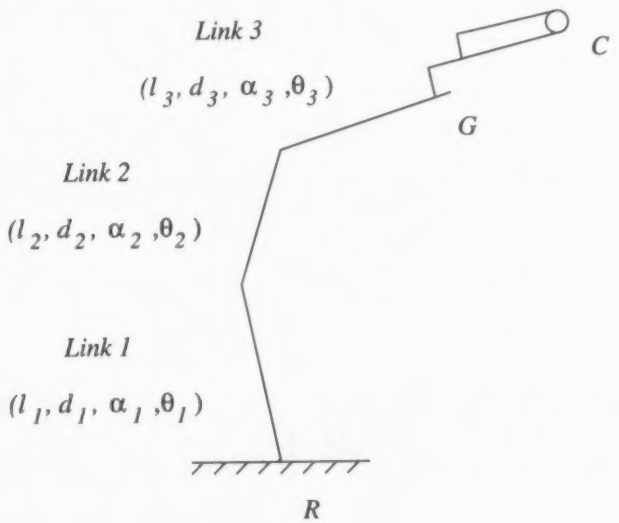

Figure 5.29: Three Link Robot.

Link	l (mm)	α (deg)	d (mm)
1	0.0	90.0	203.2
2	432.0	-90.0	0.0
3	203.2	0.0	0.0

Table 5.5: Actual Values of Link Parameters.

The encoder offsets ($\delta\theta_1$, $\delta\theta_2$, $\delta\theta_3$) were fixed at 1 degree. The value of T_{gc} was fixed and this was used to compute the link parameters. First, link 3 parameters were determined and these values were used to calibrate link 2 and link 1 by moving

one joint at a time. For different movements the camera motion (camera extrinsic calibration) was determined from equation (4.11) using the actual link parameters. These values were used to obtain the link parameters according to the calibration procedure developed in chapter 4. The angle of movement was varied from 0 to 60 deg in steps of 10, and the average of the values computed at the end of each movement was taken to obtain the final estimate of the link parameters. The movements were paired such that the angle of movement was as large as possible. First, values were obtained without noise. Then errors were introduced in the camera measurements to determine the effect on the estimates of link parameters. Table 5.6 shows the errors in the estimates of link parameters obtained without noise in the camera measurements. It can be seen that the values obtained are accurate.

Link	δl (mm)	$\delta\alpha$ (deg)	δd (mm)	$\delta\theta$
1	0.000095	0.0006	0.000044	0.0004
2	0.000095	0.0002	0.0000334	0.0001
3	0.000087	0.00004	0.000022	0.00008

Table 5.6: Errors in Values of Link Parameters.

Next errors were introduced in the camera measurements. Both translational and rotational errors were included to study the effect on the parameter estimates. Figures 5.30, 5.31 and 5.32 show the variation of error in the link parameter l of the three links with rotational errors across the x, y and z axis. The error was introduced by rotating the camera transformations around x, y and z axis by 1 to 5 deg. It can be seen that the errors are affected more by rotational errors around the x axis. This is because the equations to compute l are more dependent on these values. Also, the errors in l_1 and l_2 are more than errors in l_3 as the error is propagated along, as link 3 is calibrated first.

Figures 5.33, 5.34 and 5.35 show the variation of errors in l with translational errors. It can be seen that translational errors along x-axis have more effect, whereas errors along y and z axis are negligible.

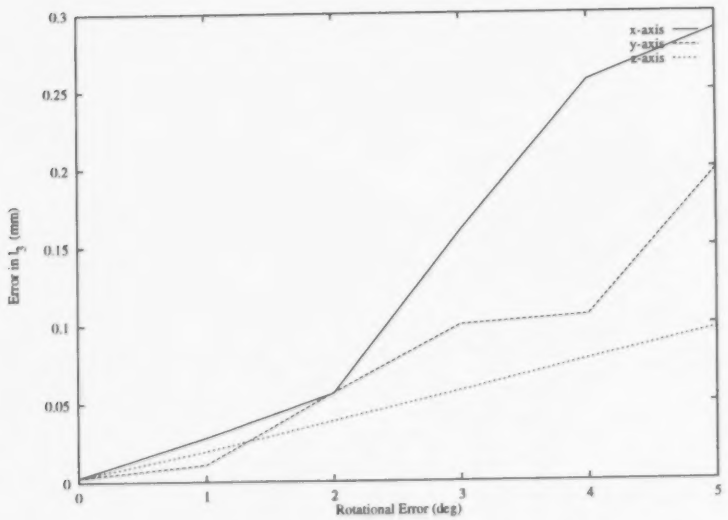

Figure 5.30: Variation of Error in l_3 with Rotational Errors.

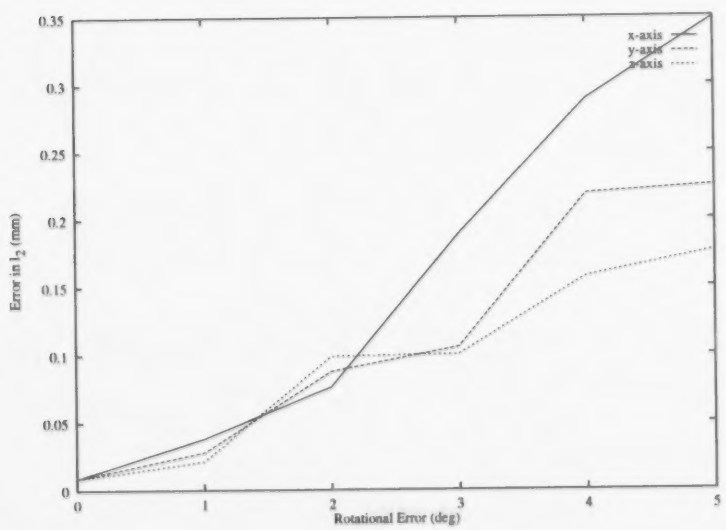

Figure 5.31: Variation of Error in l_2 with Rotational Errors.

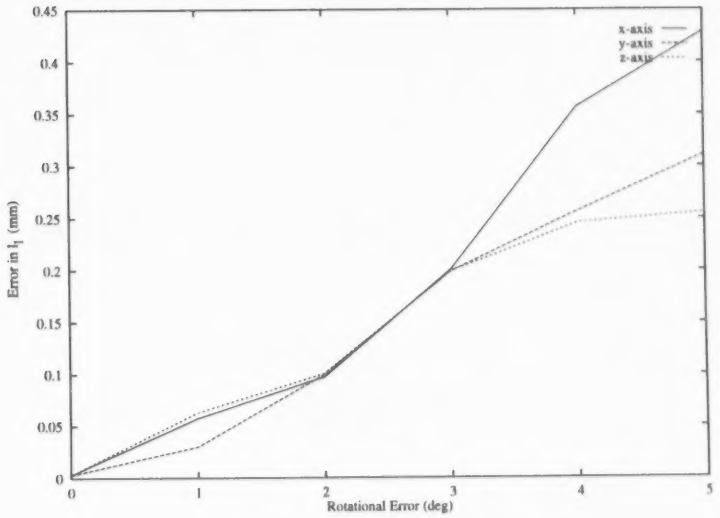

Figure 5.32: Variation of Error in l_1 with Rotational Errors.

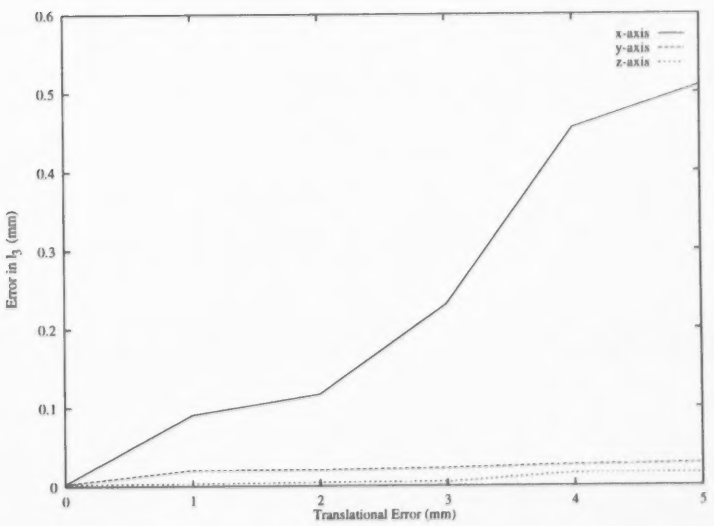

Figure 5.33: Variation of Error in l_3 with Translational Errors.

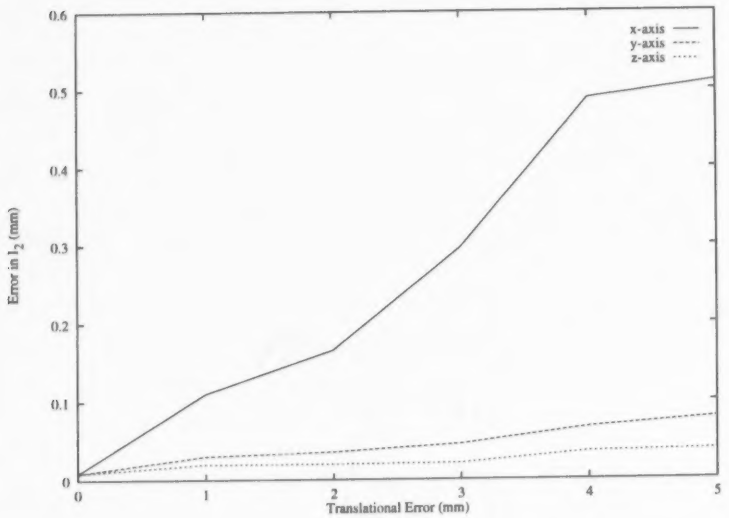

Figure 5.34: Variation of Error in l_2 with Translational Errors.

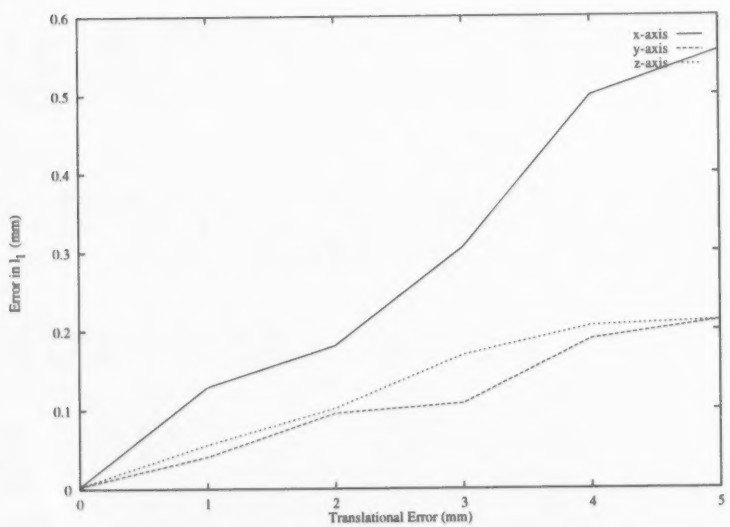

Figure 5.35: Variation of Error in l_1 with Translational Errors.

Figures 5.37 and 5.38 show the errors in the parameter d due to rotational errors, whereas figures 5.39 and 5.40 show the errors due to translational errors. It can be seen that translational errors have a more prominent effect on the estimates than rotational errors.

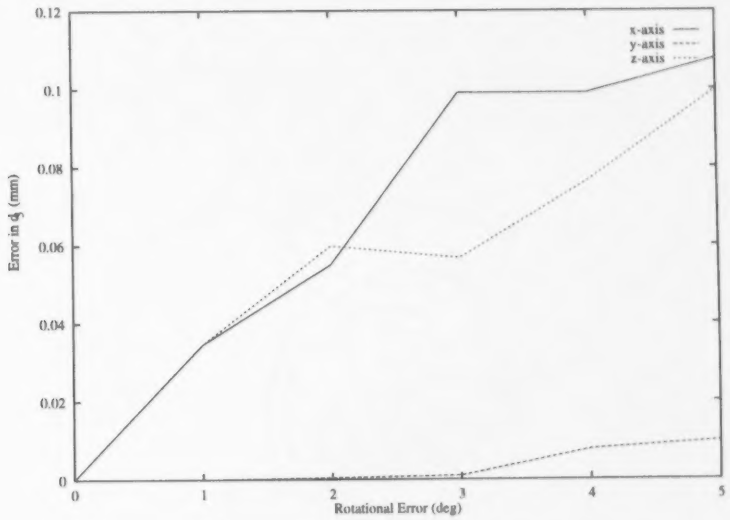

Figure 5.36: Variation of Error in d_3 with Rotational Errors.

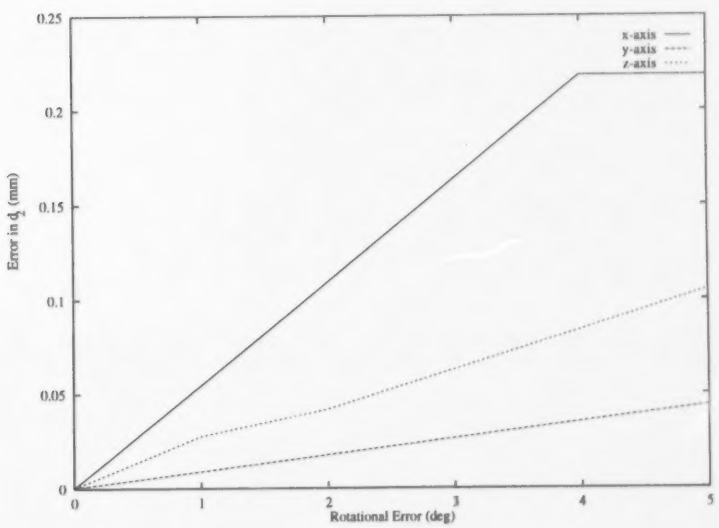

Figure 5.37: Variation of Error in d_2 with Rotational Errors.

Figures 5.40 and 5.41 show the errors in α due to rotational errors. Again, rota-

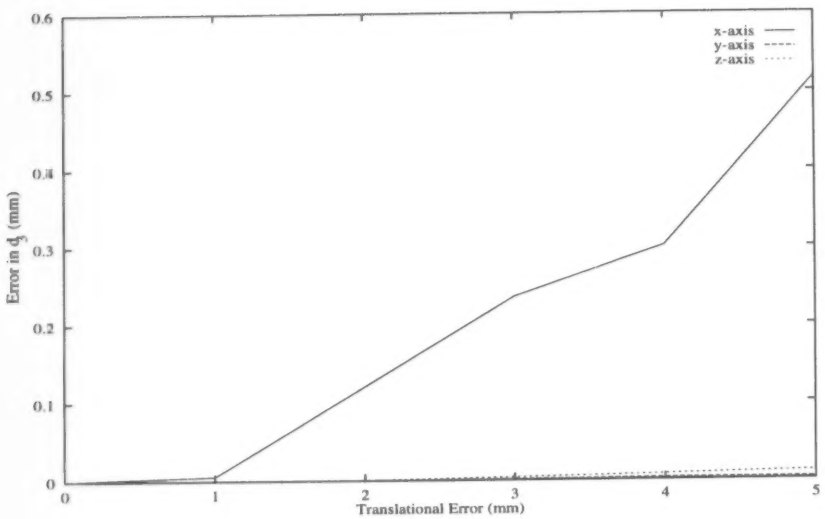

Figure 5.38: Variation of Error in d_3 with Translational Errors.

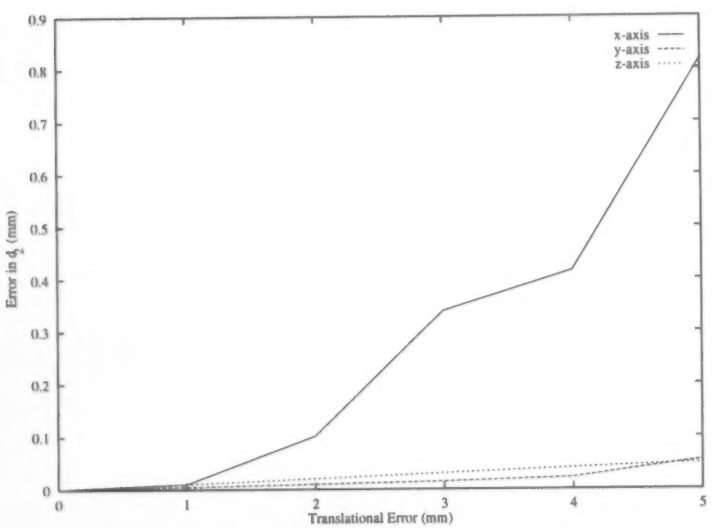

Figure 5.39: Variation of Error in d_2 with Translational Errors.

tional errors around the x axis have a larger effect as the equations are more dependent on these values. Translational errors do not have any effect on computing the estimate of α as the equations do not involve the translational components and hence are not shown.

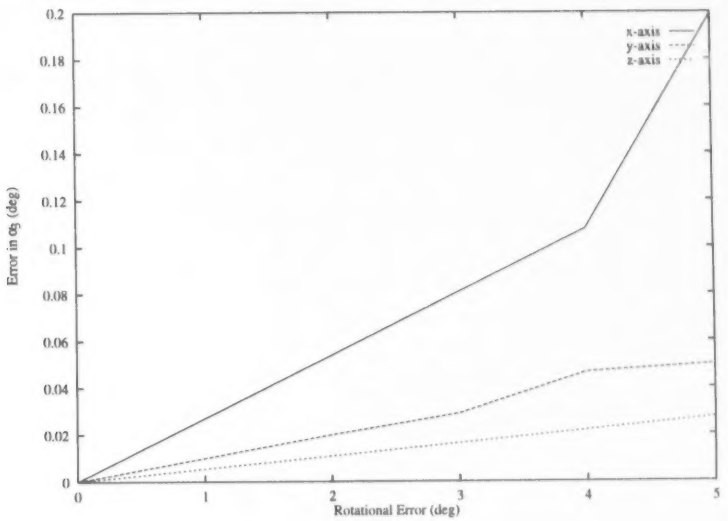

Figure 5.40: Variation of Error in α_3 with Rotational Errors.

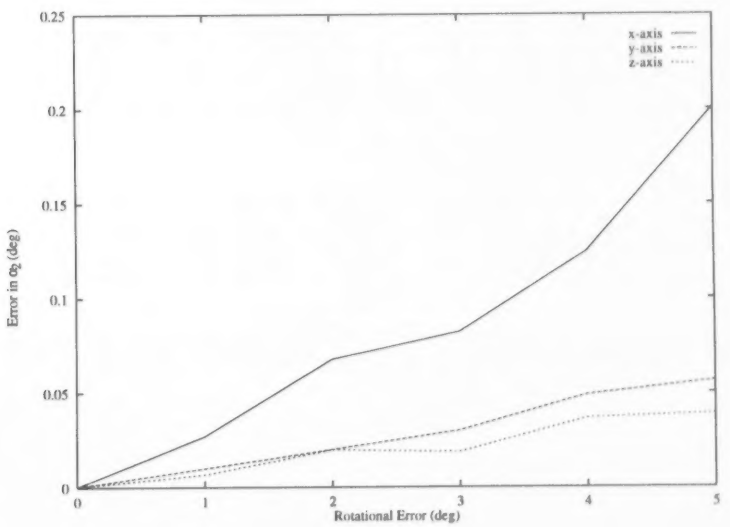

Figure 5.41: Variation of Error in α_2 with Rotational Errors.

Thus, from the above results it would appear that the robot calibration procedure

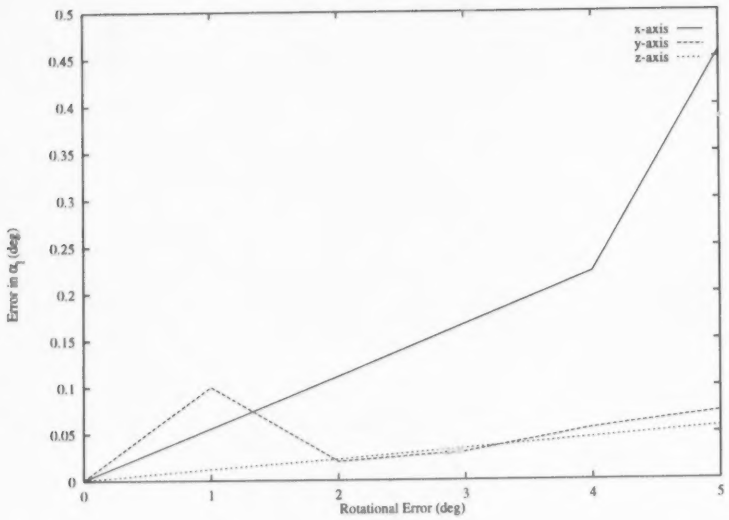

Figure 5.42: Variation of Error in α_1 with Rotational Errors.

provides reasonable estimates of the link parameters even with noisy measurements. The errors are reduced by increasing the angle of the robot joint movement, as the relative camera motion also increases, resulting in a smaller relative error.

5.3 Conclusions

This chapter presented a few experimental results of the camera and robot calibration techniques presented in Chapters 3 and 4. Experiments with synthetic and real data were conducted for the active calibration techniques. It was demonstrated that the procedures provided stable results even in the presence of noise. Simulations were done for a three link robot to illustrate the robot kinematic calibration procedure. And finally, the effect of noisy measurements on the computation of link parameters was studied.

Chapter 6

Conclusions and Future Directions

This chapter summarizes the research conducted towards the thesis and presents some conclusions and directions for further research. Advantages and disadvantages of the techniques developed are discussed. Observations concerning camera and robot manipulator calibration are presented in separate sections.

6.1 Camera Calibration

This thesis presents a novel technique for *calibrating* the *internal parameters* (focal length and image center) of a camera. We have shown that a camera capable of rotational movements (roll, pitch and yaw) can automatically calibrate itself. By considering roll movements (strategy C and D, section 3.3.2), the estimates obtained for the image center are stable. We found that larger roll movements provided more accurate estimates of the image center. The estimates of the parameters are quite robust to noise as validated by the experimental results.

6.1.1 Advantages and Limitations

The advantages of this method are as follows:

- The calibration algorithms do not require any predefined calibration pattern; scenes with stable edges are sufficient.
- The equations developed are mathematically simple.
- Internal calibration is separated from external calibration.
- Initial estimate of focal length is not required.
- Reasonable localization of contours is sufficient, no point-to-point matching is required.

One limitation of this method is that the angle of movement (rotation) of the camera has to be known. The accuracy of the calibration algorithms depends on the accuracy of the angle of rotation and the rotation axes. Another limitation is that any deviation of the pan (tilt, roll) axis from the camera x (y, z) axis would produce errors in the estimates of the camera parameters.

6.1.2 Future Directions

In this thesis, the problem of matching contours after roll movements of the camera has not been addressed. Algorithms to perform matching are necessary to automate the calibration algorithm. The corresponding contours between images can be obtained by doing correlations and searching for the best match within the region the contour is most likely to be found. The region can be computed approximately if the angle of rotation is known.

Researchers have developed models for computer-controlled zoom lenses and fish eye lenses. It will now be interesting to develop active calibration procedures for special lenses by integrating the theoretical models with the calibration algorithms

presented. The pan (tilt, roll) axis may not be parallel to the camera x (y, z) axis. Modeling of such errors would further increase the accuracy of the calibration algorithms.

6.2 Robot Calibration

The *robot calibration* technique developed uses a *vision system*, mounted on the end-effector, to obtain estimates of the parameters of the robot kinematic model. This procedure is incremental, i.e., one link is calibrated at a time, starting with the most distal link, by moving each joint. This technique assumes that the hand-to-eye transformation is known. Simulations were performed to illustrate the proposed calibration technique.

The main advantage of this technique is that, since only one link is calibrated at a time, the dimensionality of the problem is reduced. Also, the mathematical formulation involves solving linear equations only. One major drawback of this technique is that the errors are propagated along the links as the calibration is performed incrementally.

6.2.1 Issues

There are two important issues when using a vision system as a measurement mechanism: *accuracy* and *field of view* of the camera.

The accuracy of the robot calibration depends on the accuracy of the vision system. The accuracy of camera measurements depends on the camera resolution and error in image feature location. Any errors in locating the image coordinates of the calibration points would produce errors in computing the camera location. This would result in errors in the estimates of the kinematic parameters of the robot model. The accuracy obtained can be increased by using a higher resolution camera. The error

in image feature location can be reduced by using special techniques, which aim at sub-pixel accuracy, to extract the image coordinates of the calibration points. The precision of the calibration object is also important. The locations of calibration points have to be known with a reasonable accuracy to obtain more accurate camera measurements.

Another important issue in using a vision system as a measurement system is the field of view of the camera. The measurement system should be capable of operating through a large portion of the robot work space. Since, in this technique the camera is mounted on the robot manipulator, this problem is overcome to a certain extent. But since the calibration object must always be in the field of view of the camera, some movements of the manipulator may be limited. In such cases, using a large calibration object is useful.

In general, improvement in robot accuracy due to calibration is limited by the accuracy of the measurement system, as well as, inaccuracies that result due to errors which have not been modeled. This forces us to conclude that there is a limit to the accuracy of robot arm positioning.

6.2.2 Future Directions

The robot calibration technique was tested by performing simulations using synthetic data. Experiments need to be conducted to test the performance in real situations.

The model discussed in this thesis deals only with geometric parameters. But non-geometric parameters also contribute to positioning errors. There is, therefore, a need for robot models that compensate for errors caused by non-geometric parameters. It is hard to fully compensate for these errors (for example, motor parameters) however, and the models become complicated.

It would be interesting to generate a relationship between the error in image feature location and the error in the estimated kinematic parameters, and then find

the effect of the accuracy of the measurement system on the accuracy of the model parameters.

The technique developed assumes that the hand-to-eye transformation is known. The method can be extended to the case when this transformation is unknown, by starting with initial estimates of the link parameters and refining the values. Research could be done to see if it is possible to perform the robot calibration independent of this relationship [Lenz and Tsai 1989].

Performing robot calibration using arbitrary scenes instead of a fixed pattern is another interesting topic that can be explored in the future.

Bibliography

Ahmad, S. [1988]. "Analysis of Robot Drive Train Errors, Their Static Effects and Their Compensations" *IEEE Journal of Robotics and Automation*, *4*(2), 117–128.

Aloimonos, J. Y. (Ed.). [1993]. *Active Perception.* Lawrence Erlbaum Associates.

Aloimonos, J. Y., Bandyopadhay, A., and Weiss, I. [1987]. "Active Vision" In *Proceedings of International Conference on Computer Vision*, pp. 35–54.

Bani-Hashemi, A. [1992]. "A Fourier Approach to Camera Orientation" In *Proceedings of IEEE International Conference on Robotics and Automation*, pp. 1532–1538.

Basu, A. [1993]. "Active Calibration" In *Proceedings of IEEE International Conference on Robotics and Automation*, pp. 495–500.

Beardsley, P., Murray, D., and Zisserman, A. [1992]. "Camera Calibration Using Multiple Images" In *Second European Conference on Computer Vision*, pp. 312–320.

Borm, J. H. and H., M. C. [1989]. "Experimental Study of Observability of Parameter Errors in Robot Calibration" In *Proceedings of IEEE International Conference on Robotics and Automation*, pp. 587–592.

Brown, D. C. [1971]. "Close-range Camera Calibration" *Photogrammetric Engineering*, *37*, 855–866.

Caenen, J. L. and Angue, J. C. [1990]. "Identification of Geometric and Non-geometric Parameters of Robots" In *Proceedings of IEEE International Conference on Robotics and Automation*, pp. 1032–1037.

Champleboux, G., Lavallee, S., Sautot, P., and Cinquin, P. [1992]. "Accurate Calibration of Cameras and Range Imaging Sensors: The NPBS Method" In *Proceedings of IEEE International Conference on Robotics and Automation*, pp. 1552–1557.

Chang, Y. and Liang, P. [1989]. "On Recursive Calibration of Cameras for Robot Hand-Eye Systems" In *Proceedings of IEEE International Conference on Robotics and Automation*, pp. 838–843.

Chen, J. and Chao, L. M. [1986]. "Positioning Error Analysis for Robot Manipulators with All Rotary Joints" In *Proceedings of IEEE International Conference on Robotics and Automation*, pp. 1011–1016.

David, J. B., Davi, G., and John, M. H. [1991]. "Autonomous Robot Calibration for Hand-Eye Coordination" *The International Journal of Robotics Research*, *5*(10), 550–559.

Driels, M. R. and Uday, S. P. [1991]. "Vision Based Automatic Theodolite for Robot Calibration" *IEEE Transactions on Robotics and Automation*, *7*(3), 351–360.

Faig, W. [1975]. "Calibration of Close-range Photogrammetry Systems: Mathematical Formulation" *Photogrammetric Engineering*, *41*, 1479–1486.

Faugeras, O. D., Luong, Q.-T., and Maybank, S. J. [1992]. "Camera Self-Calibration: Theory and Experiments" In *Second European Conference on Computer Vision*, pp. 320–334.

Faugeras, O. D. and Toscani, G. [1986]. "The Calibration Problem for Stereo" In *Proceedings of IEEE International Conference on Computer Vision and Pattern Recognition*, pp. 15–20.

Ganapathy, S. [1984]. "Decomposition of Transformation Matrices for Robot Vision" In *Proceedings of IEEE International Conference on Robotics and Automation*, pp. 130–139.

Gennery, D. B. [1979]. "Stereo-Camera Calibration" In *Proceedins of Image Understanding Workshop*, pp. 101–108.

Gremban, K. D., Thorpe, C. E., and Kanade, T. [1988]. "Geometric Camera Calibration using Systems of Linear Equations" In *Proceedings of IEEE International Conference on Robotics and Automation*, pp. 562–567.

Hall, E. L., Tio, M. B. K., McPherson, C. A., and Sadjadi, F. A. [1982]. "Curved Surface Measurement and Recognition for Robot Vision" In *Proceedings IEEE Workshop on Industrial Applications of Machine Vision.*

Hayati, S. and Mirmirani, M. [1985]. "Improving the Absolute Positioning Accuracy of Robot Manipulators" *Robotic Systems*, *2*, 397–413.

Hayati, S., Tso, K., and Roston, G. [1988]. "Robot Geometry Calibration" In *Proceedings of IEEE International Conference on Robotics and Automation*, pp. 947–951.

Hollerbach, J. M. and Bennett, D. J. [1988]. "Automatic Kinematic Calibration Using a Motion Tracking System" In *Proceedings of 4^{th} Internation Symposium on Robotics Research*, pp. 191–198.

Horaud, R., Mohr, R., and Lorecki, B. [1992]. "Linear-Camera Calibration" In *Proceedings of IEEE International Conference on Robotics and Automation*, pp. 1539–1544.

Ishii, M. [1991]. "Kinematic Model and Calibration of a Robot Manipulator" *Advanced Robotics*, *5*(3), 337–347.

Ishii, M., Sakane, S., Kakikura, M., and Mikami, Y. [1987]. "A New Calibration System for Improving Absolute Positioning Accuracy of Robot Manipulators"

In *Proceedings of the 16th International Symposium on Industrial Robots*, pp. 1017–1025.

Izaguirre, A., Pu, P., and Summers, J. [1985]. "A New Development in Camera Calibration Calibrating a Pair of Mobile Cameras" In *Proceedings of IEEE International Conference on Robotics and Automation*, pp. 74–79.

Judd, R. P. and Knasinski, A. B. [1987]. "A Technique to Calibrate Industrial Robots with Experimental Verification" In *Proceedings of IEEE International Conference on Robotics and Automation*, pp. 351–357.

Kanatani, K. [1987]. "Camera Rotation Invariance of Image Characteristics" *Computer Vision, Graphics and Image Processing*, *39*(3), 328–354.

Kazerounian, K. and Qian, Z. G. [1990]. "Kinematic Calibration of Robotic Manipulators" In *Proceedings of ASME Design Technologies: Trends and Developments in Mechanisms, Machines and Robotics*, pp. 261–266.

Lenz, R. K. and Tsai, R. Y. [1989]. "Calibrating a Cartesian Robot with Eye-on-hand Configuration Independent of Eye-to-Hand Relationship" *IEEE Transactions on Pattern Analysis and Machine Intelligence*, *11*(9), 916–928.

Linnainmaa, S., Harwood, D., and Davis, L. S. [1988]. "Pose Determination of a Three-dimensional Object using Triangle Pairs" *IEEE Transactions on Pattern Analysis and Machine Intelligence*, *10*, 634–647.

Maragos, P. [1987]. "Tutorial on Advances in Morphological Image Processing and Analysis" *Optical Engineering*, *26*(7), 623–632.

Martins, H. A., Birk, J. R., and Kelley, R. B. [1981]. "Camera Models Based on Data from Two Calibration Planes" *Computer Graphics and Image Processing*, *17*, 173–180.

McKerrow, P. J. [1990]. *Introduction to Robotics.* Addison-Wesley Publishing Company.

Nowrouzi, A., Kavina, Y. B., Kochekali, H., and Whitaker, R. A. [1988]. "An Overview of Robot Calibration Techniques" *The Industrial Robot*, *15*, 229–232.

Okamoto, A. [1981]. "Orientation and Construction of Models, Part I: The Orientation Problem in Close-range Photogrammetry" *Photogrammetric Engineering and Remote Sensing*, *47*, 1437–1454.

Preising, B. and Hsai, T. C. [1991]. "Robot Performance Measurement and Calibration using a 3D Computer Vision System" In *Proceedings of IEEE International Confereence on Robotics and Automation*, pp. 2079–2084.

Puskorius, G. V. and Feldkamp, L. A. [1987]. "Global Calibration of a Robot/Vision System" In *Proceedings of IEEE International Conference on Robotics and Automation*, pp. 190–195.

Renders, J.-M., Rossignol, E., Becquet, M., and Hanus, R. [1991]. "Kinematic Calibration and Geometrical Parameter Identification of Robots" *IEEE Transactions on Robotics and Automation*, 7(6), 721–732.

Roth, Z. S., Zhuang, H., and Wang, L. [1987]. "Simultaneous Calibration of a Robot and a Hand-Mounted Camera" In *Proceedings of IEEE International Conference on Robotics and Automation*, pp. 149–154.

Shiu, Y. C. and Ahmad, S. [1989]. "Calibration of Wrist-Mounted Robotic Sensors by Solving Homogeneous Transform Equations of the Form AX = XB" *IEEE Transactions on Robotics and Automation*, *5*(1), 16–29.

Slama, C. C. (Ed.). [1980]. *Manual of Photogrammetry.* American Society of Photogrammetry.

Sobel, I. [1974]. "On Calibrating Computer Controlled Cameras for Perceiving 3D Scenes" *Artificial Intelligence*, *5*, 185–198.

Stone, H. W. [1987]. *Kinematic Modelling, Identification, and Control of Robotic Manipulators.* Kluwer Academic Publishers.

Strat, T. M. [1984]. "Recovering the Camera Parameters from a Transformation Matrix" In *Proceedings of Image Understanding Workshop*, pp. 264–271.

Sutherland, I. [1974]. "Three-dimensional Data Input by Tablet" *Proceedings of the IEEE, 62*, 453–461.

Tsai, R. Y. [1987]. "A Versatile Camera Calibration Technique for High Accuracy 3D Machine Vision Metrology Using Off-the-Shelf TV Cameras and Lenses" *IEEE Journal of Robotics and Automation, 3*(4), 323–346.

Tsai, R. Y. and Lenz, R. K. [1988]. "Techniques for Calibration of the Scale Factor and Image Center for High Accuracy 3D Machine Vision Metrology" *IEEE Transactions on Pattern Analysis and Machine Intelligence, 10*(5), 713–720.

Tsai, R. Y. and Lenz, R. K. [1989]. "A New Technique for Fully Autonomous and Efficient 3D Robotics Hand/Eye Calibration" *IEEE Transactions on Robotics and Automation, 5*(3), 345–358.

Turk, M. A., Morgenthaler, D. G., Gremban, K. D., and Marra, M. [1987]. "Video Road-Following for the Autonomous Land Vehicle" In *Proceedings of IEEE International Conference on Robotics and Automation*, pp. 273–280.

Vietschegger, W. K. and Wu, C.-H. [1988]. "Robot Calibration and Compensation" *IEEE Journal of Robotics and Automation, 4*(6), 643–656.

Wei, G.-Q., He, Z., and Ma, S. D. [1989]. "Camera Calibration by Vanishing Point and Cross Ratio" In *Proceedings of IEEE International Conference on Acoustics, Speech and Signal Processing*, pp. 1630–1633.

Wei, G.-Q. and Ma, S. D. [1991]. "Two Plane Camera Calibration: A Unified Model" In *Proceedings of IEEE International Conference on Robotics and Automation*, pp. 133–138.

Whitney, D. E., Lozinski, C. A., and Rourke, J. M. [1984]. "Industrial Robot Calibration Method and Results" In *Proceedings of 1984 International Computers in Engineering Conference and Exhibition*, pp. 92–100.

William, I. G. and Louis, A. T. [1987]. "A Unified Approach to the Linear Camera Calibration Problem" In *Proceedings of IEEE International Conference on Computer Vision*, pp. 511–515.

Wilson, R. G. and Shafer, S. A. [1993]. "What is the Center of the Image?" Tech. rep. CMU-CS-93-122, School of Computer Science, Carnegie Mellon Univ.

Wong, K. W. [1975]. "Mathematical Formulation and Digital Analysis in Close-range Photogrammetry" *Photogrammetric Engineering and Remote Sensing*, *41*, 1355–1373.

Yakimovsky, Y. and Cunningham, R. [1978]. "A System for Extracting Three-dimensional Measurements from a Stereo Pair of TV Cameras" *Computer Graphics and Image Processing*, *7*, 195–210.

Zak, G., Fenton, R. G., and Benhabib, B. [1993]. "A Simulation Technique for the Improvement of Robot Calibration" *Journal of Mechanical Design*, *115*(3), 674–679.

Zeigert, J. and Datseris, P. [1988]. "Basic Considerations for Robot Calibration" In *Proceedings of IEEE International Conference on Robotics and Automation*, pp. 932–938.